SOLUBILITIES AND MASS TRANSFER COEFFICIENTS OF GASES IN SILICONE OIL AND POLYALPHAOLEFIN

by

Dinara Abdrakhimova

B.S. Petroleum Engineering, Kazakh National Technical University, 2011

Submitted to the Graduate Faculty of

The Swanson School of Engineering in partial fulfillment

of the requirements for the degree of

Master of Science in Petroleum Engineering

University of Pittsburgh

2015

UNIVERSITY OF PITTSBURGH

SWANSON SCHOOL OF ENGINEERING

This thesis was presented

by

Dinara Abdrakhimova

It was defended on

April 2nd, 2015

and approved by

George E. Klinzing, Ph.D., Professor, Department of Chemical and Petroleum Engineering

Shiao-Hung Chiang, Ph.D., Professor, Department of Chemical and Petroleum Engineering

Thesis Advisor: Badie I. Morsi, Ph.D., Professor, Department of Chemical and Petroleum Engineering

SOLUBILITIES AND MASS TRANSFER COEFFICIENTS OF GASES IN SILICONE OIL AND POLYALPHAOLEFIN

Dinara Abdrakhimova, M.S.

University of Pittsburgh, 2015

The equilibrium solubilities (C*) and volumetric liquid-side mass transfer coefficients (k_La) for He and N_2, as surrogates to H_2 and CO, and their mixtures were measured in a Silicone Oil and a SpectraSyn Polyalphaolefin as startup liquids in Fischer-Tropsch Slurry Bubble Column Reactors (SBCRs). The data were obtained within wide ranges of pressures (4-30 bar), temperatures (298-398 K) and mixing speeds (1000-1400 rpm) in one-gallon agitated ZipperClave reactor operating in the gas-inducing mode. The effects of different operating variables as well as the gas and liquid natures on C* and k_La for He and N_2 in the two liquids were discussed. The interpretation of the experimental results and calculations reveals the following:

- At constant temperature, the C* values of He and N_2 in the Silicone Oil and SpectraSyn polyalphaolefin increased non-linearly with the gas partial pressure and hence Henry's Law was not applicable.
- Under similar pressures and temperatures, the C* values of both gases in the Silicone Oil were greater than those in the SpectraSyn polyalphaolefin; and C* values of N_2 were greater

than those of He in both liquids. This behavior was attributed to the differences among the Hildebrand solubility parameters calculated for the gases and liquids used.

- The k_La values of both gases in the two liquids increased with the mixing speed, gas partial pressure and system temperature which was related to the increase of both the gas-liquid interfacial area (a) and the liquid-side mass transfer coefficient (k_L). Increasing mixing speed, gas partial pressure and system temperature increased the gas holdup and decreased the liquid-phase viscosity and surface tension, leading to the formation of small gas bubbles and hence an increase of (a). Also, increasing mixing speed and system temperature increased the turbulence and the gas diffusivity in the liquid, resulting in an increase of (k_L).
- Under similar pressure, temperature and mixing speed, the k_La values of He in the two liquids were greater than those of N_2. This behavior was because at the same temperature the diffusivities of He in both liquids were greater than those of N_2 and hence $(k_L)_{He}$ and consequently $(k_La)_{He}$ values were greater than those of N_2 in both liquids, knowing that $k_L \propto (D_{AB})^n$, n =1 for the two-film theory and 0.5 for the penetration theory.
- Unlike gas solubilities, k_La values of He were lower in Silicone Oil than those in the SpectraSyn Polyalphaolefin, whereas the opposite was true in the case of N_2. This behavior was attributed to the lower He and N_2 diffusivities in Silicone Oil than in the SpectraSyn Polyalphaolefin, resulting in small k_L values for both gases. On the other hand, the higher viscosity of Silicone Oil than that of the SpectraSyn Polyalphaolefin was expected to enhance the formation of large bubbles with small gas-liquid interfacial area (a). This was true in the case of the light He where smaller k_L and, a values in the more viscous liquid (Silicone Oil) resulted in lower k_La values. In the case of N_2, however, it seems that the induced heavy N_2 bubbles were broken by the impeller and scattered throughout the reactor,

leading to the formation of small bubbles with large gas-liquid interfacial area (a). Thus, the small k_L values of N_2 in the more viscous liquid (Silicone Oil) were overcame by its larger a values, leading to the higher k_La than those in the less viscous (SpectraSyn polyalphaolefin).

- Five liquids, namely Silicone oil, SpectraSyn polyalphaolefin, reactor wax, n-tetradecane and paraffins mixture, were explored as potential startup liquids for the F-T synthesis in SBCRs at 410 K and 15 bars at two α values, 0.85 and 0.92. This investigation indicated that the SpectraSyn polyalphaolefin cloud remain in the reactor for over 200 hr, whereas the paraffins mixture would remain only for about 100 hr. This behavior was related to the startup liquid molecular weight, which was the main factor controlling its residence time in the SBCRs.

TABLE OF CONTENTS

LIST OF TABLES

LIST OF FIGURES

NOMENCLATURE

a	Gas-liquid interfacial area per unit liquid volume, m^{-1}
C^*	Solubility of the gas at equilibrium, mol m^{-3}
C_L	Concentration of the gas in the liquid bulk, mol m^{-3}
D_{AB}	Mutual diffusion coefficient of solute A in solvent B, m^2 s^{-1}
g	Gravitational constant, m^2 s^{-1}
He	Henry's law constant, bar m^3 $kmol^{-1}$
H_V	Molar heat of vaporization, $J.mol^{-1}$
i	Carbon number, -
k	Phase mass transfer coefficient, m s^{-1}
MW	Phase molecular weight, kg $kmol^{-1}$
N	Mixing speed, rpm
P	Pressure, bar
P_c	Critical pressure, bar
P^v	Saturated vapor pressure of the liquid, bar
R	Universal gas constant, $kJ.kmol^{-1}.K^{-1}$
T	Temperature, K
t	Time, s
T_b	Boiling point, K
T_c	Critical temperature, K
T_r	Reduced temperature, -
v_A	Molar volume of solute A at its normal boiling point temperature, m^3 $kmol^{-1}$
V_c	Critical volume, m^3 $kmol^{-1}$
V_G	Volume of the gas phase, m^3
V_L	Volume of the liquid phase, m^3
w_i	Mass fraction of component *i*, -
x_i	Mole fraction of component *i* in the liquid phase, -
y_i	Mole fraction of component *i* in the gas phase, -

Z_c	Critical compressibility, -

Greek symbols

α	Anderson-Schulz-Flory (ASF) chain growth probability distributions, -
δ_i	Solubility parameter of phase *I*, $(MPa)^{0.5}$
μ	Phase viscosity, kg m^{-1} s^{-1}
ν	Kinematic viscosity, m^2/s
ρ	Density, kg m^3
σ_L	Surface tension of the liquid, N m^{-1}

Subscripts

A	Solute
avg.	Average
B	Solvent
eq.	Equilibrium
F	Final
G	Gas phase
I	Initial
L	Liquid phase
m	Mixture
pre	Preheater
V	Vapor phase

Abbreviations and acronyms

bbl	barrel
CTL	Coal-to-Liquid
F-T	Fischer-Tropsch
GIR	Gas Inducing Reactor
GTL	Gas-to-Liquid
TD	Tank diameter
TV	Tank volume
WGS	Water Gas Shift

ACKNOWLEDGEMENTS

I would like to express my sincere gratitude to my advisor Professor Badie I. Morsi during my participation in this research project and in the preparation of this thesis. I am grateful to Professor Shaio-Hung Chiang and George E. Klinzing for serving at my committee.

I do appreciate the exceptional cooperation of my labmates: Mr. Omar Basha, Dr. Laurent Sehabiague, Ms. Fabiana Arias, Mr. Yongtai Li, and Mr. Pedro Rosa. I consider it an honor to have worked with all of them.

My deepest gratitude goes to my parents. It is a great pleasure to thank all my friends for their extensive support and encouragement throughout this endeavor.

Last but not the least, I would like to acknowledge the scholarship support I have received from JSC "Center for International Programs."

1.0 INTRODUCTION

In 2013, the US oil production, consumption and net imports were 10.0, 18.9 and 7.7 million bbl/day, respectively, with 90% of the oil produced was used in the transportation sector [1]. The political instability in oil producing countries, such as the Middle East, Venezuela, and Nigeria, coupled with the ever increasing worldwide demand for crude oil, have led to a very unpredictable oil market, with prices fluctuating between $120 and $40 a barrel over the past 10 years, as shown in Figure 1-1. Unfortunately, such instability in the oil market is expected to continue throughout the world in the near future. In the US, the volatility of the crude oil and transportation fuels prices is creating an urgent need for energy independence through other alternative energy sources. Although the new Marcellus shale gas plays are projected to be lucrative energy sources, their development and gas production are still at the inception stage and are unable so far to satisfy the increasing energy demands, particularly in the transportation sector. Synthetic chemicals and fuels produced through the Fischer-Tropsch (F-T) technology, however, are considered one of the main viable solutions for such an increasing demand, due to the availability of abundant F-T feedstock. In 2013, the US had huge proven natural gas reserves of 330 trillion ft^3 and coal reserves totaling 237 billion tons, representing 26.6% of the total world's proved reserves [1]. Also, the US has considerable biomass feedstocks with an increasing projected availability in the future [2], in addition to heavy vacuum residue, which is available in all the US refineries. These feedstocks can all be converted to synthetic chemicals

and fuels through Fischer-Tropsch (F-T) synthesis via Gas-To-Liquid (GTL), Coal-To-Liquid (CTL) and Biomass-To-Liquid (BTL) processes.

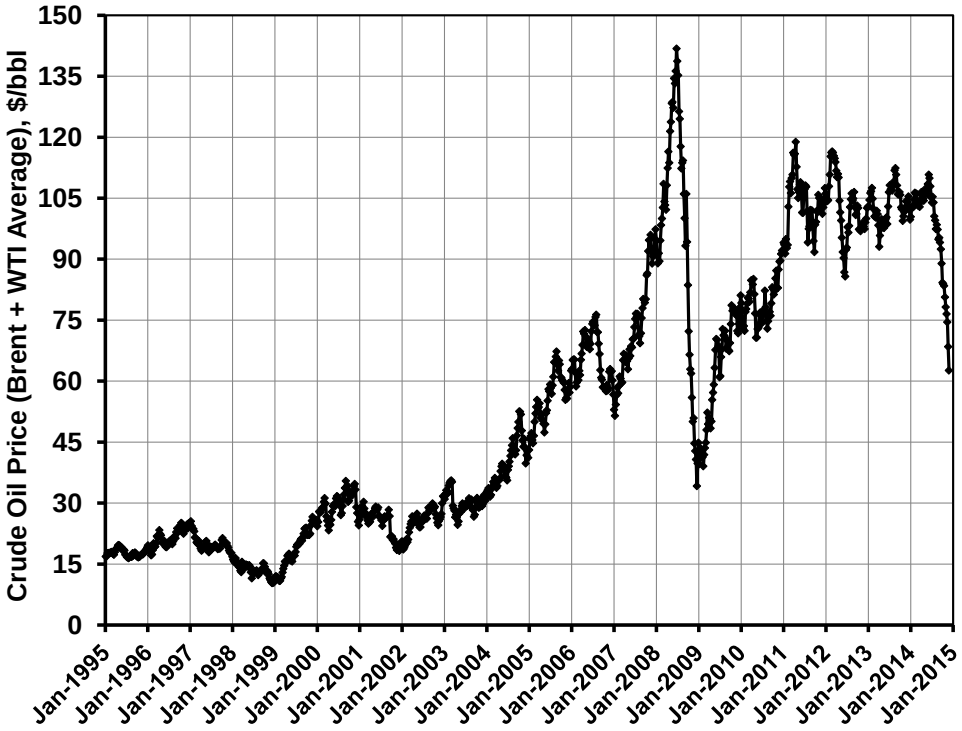

Figure 1-1: : Crude oil prices over the past 20 years [3]

It should be mentioned that research and development in the F-T synthesis had been primarily driven by strategic rather than economic reasons. For instance, F-T synthesis was developed in Germany during World War II and in South Africa during the apartheid era. In recent decades, however, there has been a growing interest in F-T technologies as a crude oil substitute for the production of fuels and other petrochemical products. In fact, F-T synthesis has been applied on a large scale in South Africa, Malaysia and Qatar; however, its worldwide commercialization has been hampered by its relatively high operating and maintenance costs and the volatility of the global crude oil prices. Nonetheless, the current and projected hikes in the oil prices have

renewed interest in the implementation of the F-T technology. In 2001-2004, the F-T synthesis was projected to be economically feasible, if crude oil prices were about 20-24$/bbl [4-6]. In 2011, however, Liu et al. [7] projected that the F-T synthesis would be viable at oil prices of $59-65/bbl.

2.0 BACKGROUND

2.1 THE FISCHER-TROPSCH SYNTHESIS PROCESS

The F-T synthesis process enables the conversion of carbon containing sources, such as natural gas, coal and biomass into synthetic liquid fuels and high value chemicals. The F-T synthesis was developed in the 1920's by Franz Fischer and Hans Tropsch in Germany [8-12], with the intent of producing synthetic hydrocarbons. Subsequently, by 1938 there were nine F-T plants operating in Germany with a total capacity of around 13,200 bpd [10]. The F-T process developments continued in South Africa during the Apartheid period, with multiple Coal to Liquid (CTL) plants developed by Sasol. Gas-to-liquid (GTL) plant were also built by Sasol (South Africa) and Shell (Malaysia). Furthermore, industrial applications and developments in the F-T area continued over the past decade, spearheaded primarily by Sasol and Shell as they recently commissioned in Qatar the largest F-T Slurry Bubble Column Reactor (SBCR) and multitubular Fixed-bed Reactor (FBR), respectively [13-15].

During the F-T synthesis, the syngas ($CO + H_2$) reacts in the presence of a heterogeneous catalyst to produce a wide variety of hydrocarbon products, primarily linear alkanes and alkenes. Iron (FeOx) and cobalt (Co) catalysts are typically used in the commercial scale F-T applications [14, 16]. Iron catalyst is cheap and has a high water-gas-shift (WGS) activity. It is prone, however, to severe attrition and the water produced by the F-T reaction appeared to decrease its

activity [10, 17]. Cobalt-based catalyst, on the other hand, has higher activity since it is not strongly inhibited by water. It also has longer life than iron catalyst as it is more resistant to attrition. Cobalt-based catalyst, however, is more expensive and has no WGS activity [10, 18].

During Cobalt catalyzed F-T reaction, the oxygen from CO dissociation is converted to H_2O, as shown in Equation (2-1). Conversely, iron catalyst has a high affinity for the WGS reaction as shown in Equation (2-2), resulting in the conversion of a significant portion of the oxygen from CO dissociation into CO_2.

$$\text{F} - \text{T:} \qquad CO + 2H_2 \rightarrow \ -CH_2- \ + \ H_2O \tag{2-1}$$

$$\text{WGS:} \qquad CO + H_2O \leftrightarrows H_2 + \ CO_2 \tag{2-2}$$

Depending on the reaction temperature, the F-T process is referred to as low temperature F-T (LTFT) or high temperature F-T (HTFT). The temperature of the LTFT ranges from 180 to 260 ^{o}C and the syncrude produced is wax consisting mostly of long chain hydrocarbons, while the temperature of the HTFT process is between 290 and 360 ^{o}C and the products are mostly short chain hydrocarbons and gases. Thus, the final products of the LTFT process consist mostly of diesel fuel, while gasoline production has been the focus of the HTFT [9]. The LTFT syncrude is easy to upgrade by a hydroprocessing step and a fractionation step to obtain naphtha and middle distillate, whereas the HTFT syncrude requires more complex refinery facilities [9]. It should be noted that recent R&D and commercial efforts have been focused on the LTFT due to the current drive for using more diesel engines than gasoline engines, the excellent quality of sulfur-free F-T diesel, and perhaps the mild conditions of the process.

In multi-tubular FBRs, the syngas flows through small diameter tubes packed with catalyst at small voidage, resulting in a high pressure drop and an increased operating cost. These reactors have comparatively complex heat transfer characteristics and their maximum production capacity

is limited by the amount of heat which can be removed. SBCRs, on the other hand, have a simpler design and allow for much higher heat removal efficiencies than multi-tubular FBRs due to the presence of a large volume of the liquid-phase. However, the high mechanical shear on the catalyst resulting in particles attrition and the lack of a reliable system for the fine particles separation from the liquid products, have delayed commercial deployment of SBCRs until the 1990's.

Generally, the F-T process includes three main steps: syngas generation, F-T catalytic reactions and product upgrading as shown in Figure 2-1. The syngas generation involves converting the carbon containing feedstock into syngas (H_2 and CO mixture) via reactions with steam and optionally oxygen or air. Natural gas is converted to syngas in a reformer using either partial oxidation (POX), steam methane reforming (SMR) or auto-thermal reforming (ATR). Solid feedstocks, such as coal and biomass, however, are converted in a gasifier, of which various types have been already in industrial applications [19]. Different gasification processes and technologies have also been discussed in the literature [11, 14, 20-29].

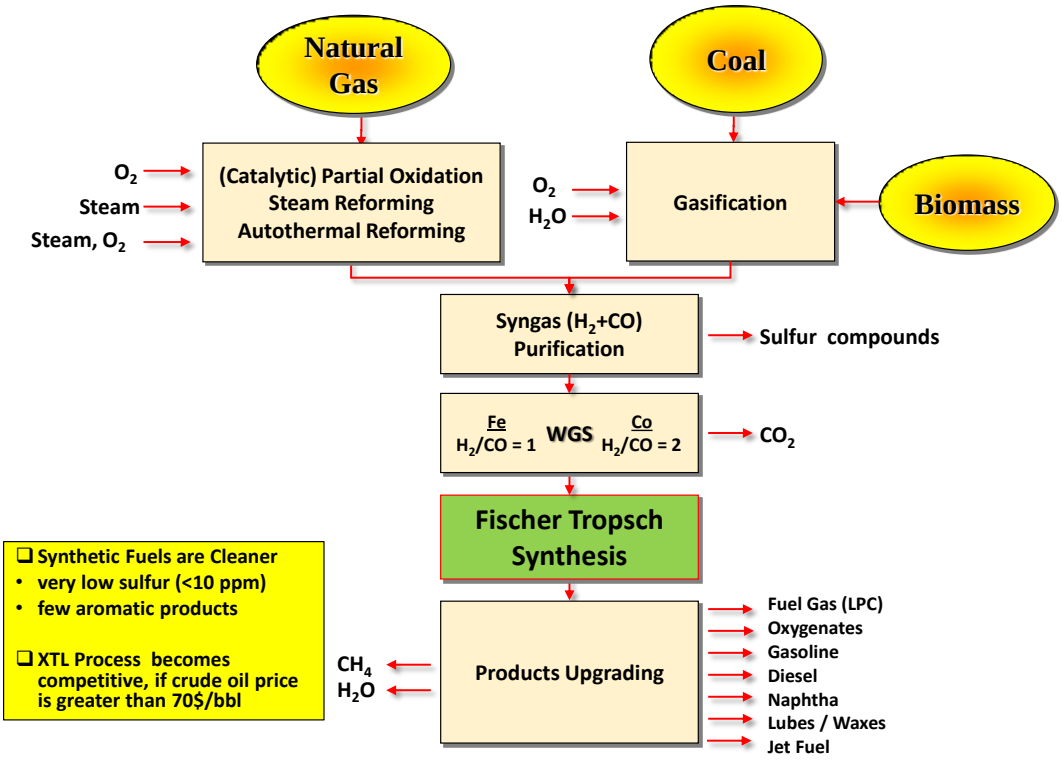

Figure 2-1: F-T process Overview (Reproduced from [30])

One of the main challenges in operating a SBCR is the startup step. Generally, this crucial step is accomplished by filling the reactor with a liquid having stable thermal and chemical properties and can stand high-pressure, high temperatures in the presence of catalyst. A polyalpha-carbon is often considered a good candidate as it would blend with the synthetic liquid products of the F-T synthesis without dramatically changing their physical or chemical properties. The H_2 and CO are simultaneously injected from the bottom of the reactor via the distributor in this liquid in order to react on the active catalyst sites. Thus, H_2 and CO should transfer through the startup fluid before their reaction on the solid catalyst in the reactor.

2.2 STARTUP LIQUIDS FOR F-T SYNTHESIS IN SBCRs

According to Pandyala et al. [31] startup liquids with different molecular weights may affect the mass and heat transfer during F-T synthesis. A lighter liquid may offer better mass transfer than a heavier one, but it may escape faster from the SBCR in the vapor-phase. At a high gas space velocity and a relatively high temperature, the slurry level can rapidly decrease, if a light liquid is used, leading to a rapid decrease in the syngas conversion. Pandyala et al. [31] also found out that in the case of iron catalyst, the conversion was independent of the molecular weight of the startup liquid, whereas it decreased in the case of cobalt catalyst.

Satterfield and Stenger [32] presented the effect of liquid composition on the performance of a fused magnetite catalyst for F-T slurry synthesis. They observed that the catalyst performed well in phenanthrene, n-octacosane and triphenylmethane, but it deactivated rapidly in Fomblin YR. According to these authors, the reaction rate in a given liquid depends on the difference between the solubility parameters not only between the liquid and reactants, but also between the liquid and activated complex. Moreover, they tried using silicone oil as a startup liquid; however, they terminated their experiments after 24 hours because the Silicone oil cracked to form water and low molecular weight silanes, which resulted in a rapid loss in catalyst activity. Davis et al. [33] reported that catalyst deactivation appeared faster in a heavy wax (Allied AC-1702) as the starting liquid than in a lighter wax (n-octacosane).

Air Products conducted tests in a 22.5-in diameter 28.3-ft high SBCR using the low-alpha catalyst UCI-1185-149 [34]. Initially, they used a C_{30} wax (Drakoil 10) as the startup liquid and then added another wax (Ethylflo-164) during the startup process. They also tested a high alpha catalyst and observed that the product wax was ultimately replaced by the startup liquid until a

heavy wax of carbon number C_{61} appeared in the reactor [35]. Mobil reported that startup liquid (Vestowax) with a molecular weight of 600 kg/kmol led to higher gas holdups when compared with that when using high molecular weight F-T product wax [34]. These observations, however, are in contrast to those by Jager [34] who reported no effect of the molecular weight of the startup liquid in a slurry phase reactor operating at 210-250 °C using a high-alpha catalyst.

Furthermore, The solubilities and gas-liquid mass transfer coefficients of H_2 and CO in three different fractions of an F-T products, with carbon numbers C_8, C_{14}, and $C_{26,}$ were measured under high-pressure and high-temperatures in non-reacting systems [36-40]. These authors concluded that the solubilities decreased with increasing carbon number and k_La values appeared to depend on the molecular weight of the F-T fraction and the amount of water dissolved in it. Thus, some effect of syngas solubilities on its conversion might be expected [34]. However, syngas conversions in different waxes were not greatly affected by the solubility in the first 10 days, but rather later on [36-38]. Therefore, an explanation based on the solubility alone is ruled out, since this would be expected to lower the conversion in high molecular weight waxes (C_{28+}) during the entire experiment, not simply during the later days [34].

Gormley et al. [34] studied the effect of the startup liquid on a low-alpha iron F-T synthesis catalyst and found that the startup liquid had little effect on the initial conversion rate, but a major effect on the rate of deactivation, which was in disagreement with the findings by Pandyala et al. [31]. Gormley et al. [34] stated that the deactivation may be related to the formation heavier hydrocarbon products from the heavier initial wax. As these products build up over time, they could restrict pore diffusion in several ways: first, of CO and H_2 into the pores, second of products out of the pores, and third of water vapor away from the catalyst surface. Inga and Morsi [41, 42] and Iglesias et al. [43] each noted that CO is more likely than H_2 to be a

limiting reactant, due to the iron catalyst high WGS activity. Akgerman and Co-workers [44-46] calculated the diffusion coefficients of reactants and products in different waxes at ambient temperatures and pressure. They reported that for the light F-T wax of average carbon number C_{29}, the diffusivities of F-T products: n-octane, n-dodecane, and n-hexadecane were 60% to 75% lower than in n-eicosane with carbon number C_{20}. Moreover, they observed that for heavy waxes with carbon number greater than C_{30}, secondary reactions of the product waxes could cause high molecular weight products to form in the pores of the catalyst, which could build up over time and restrict the diffusion of products out of the pores, thus slowing down the reaction. Previous studies on F-T startup liquids in SBCRs are summarized in Table 2-1.

In this study, the solubility and mass transfer coefficients for N_2 and He as surrogated to CO and H_2 gases in two different liquids, which could be used as a startup fluids in SBCRs (SpectraSyn and Silicone oil). The experiments are conducted in a small volume agitated reactor in order to ensure reliability and reproducibility of the experimental data in a well-controlled reactor operating under high pressures and temperatures.

Table 2-1: Previous Studies on F-T Startup Liquids in SBCRs

Startup liquid	Conditions	Comments/Conclusions	Reference
n-octacosane ($C_{28}H_{58}$) Fomblin YR (perfluoropolyether) Phanthrene Triphenylmethane	T: 234-269 ^{o}C P: 0.79-1.48 MPa Finely ground fused magnetite catalyst 1-L Autoclave	They observed that the catalyst performed well in phenanthrene, n-octacosane, and triphenylmethane, but it deactivated rapidly in Fomblin YR. According to these authors the reaction rate in a given solvent depends on the difference between the solubility parameters not only between the solvent and reactants, between the solvent and activated complex. Also, they used silicone oil as a startup solvent; however, they terminated their experiments after 24 hours because the Silicone oil cracked to form water and low molecular weight silanes, resulting in a rapid loss in catalyst activity.	Satterfield and Stenger [32]
C_{30} oil, Polywax-500, Polywax-2000, Polywax-3000	For iron based catalyst: T = 270 ^{o}C, P =13 atm, H_2/CO = 0.7 For cobalt based catalyst: T=220 ^{o}C, P = 20 atm, H_2/CO = 2	Higher conversion and lower deactivation rate were found with lower molecular weight solvents	Pandyala et al. [31]
n-Octacosane ($C_{28}H_{58}$) Polywax-655 Mobil-FT WAX Distilled allied-AC-1702	low alpha iron catalyst at 9% and 19% catalyst, flow rate of 2.4 L syngas/g-Fe h	The startup liquid has a minor effect on the catalyst's initial activity; however it has a major effect on the deactivation rate. The catalyst deactivation rate is typically accompanied with an increase in water production.	Gormley et al. [34]
$C_{28}H_{58}$, $C_{36}H_{74}$, SASOL Arge wax, MOBIL-CT-256-7 F-T wax	Gases: H_2, CO, CH_4, CO_2, C_2H_6 300 ^{o}C, 2.03 MPa	Solubilities of the gases decreased with the increase of molecular weight of the wax	Chao and Lin, taken from [34]
Olefin/Paraffin ratio	Short-term and long-term experiments; conditions as at LTFT; a supported cobalt catalyst with 10% Co/90% TiO_2	No conclusive effect of the startup liquid on the catalyst activity or deactivation rate could be reached.	Lu et al.[47]

Table 2-1 (continued).

Startup liquid	Conditions	Comments/Conclusions	Reference
F-T 200 Vestowax (MW: 600 g/mol)	T: 260-282 ^{o}C P: 1.14 – 1.83 MPa u_g: 1-3.2 cm/s H_2/CO: 0.6-1.2 5.1 cm diameter, 762 cm high bench scale SBCR reactor	The performance of FT-200 Vestowax as a startup liquid was compared to FT-slurry with 2.2 wt% catalyst formed after 61 days on stream from the same reactor. The FT-slurry showed similar behavior to the FT-200 Vestowax except that the slop of the gas holdup versus the gas velocity at low velocities is slightly larger than that of the FT-200 Vestowax. Foaming was also observed with increasing gas velocity, causing a large rise in the gas holdup. The gas holdup subsequently leveled off and slugging occurred.	Mobil [34]
Allied-AC 1702 (C_{42+} Wax)	-	Reported that catalyst deactivation appeared faster in a heavy wax (Allied AC-1702) as the starting medium than in a lighter wax (n-octacosane).	Davis et al. [33]
Drakoil 10 (C_{30} wax) Ethylflo-164	T: 210-250 ^{o}C P: 520-710 psig H_2/CO: 0.65-2.07 u_g: 0.31-0.73 cm/s Low-alpha Fe catalyst (UCI-1185-149) 22.5 in diameter 28.3 ft high SBCR	They observed that the product wax ultimately replaced the startup liquid when using a high-alpha catalyst, until a heavy wax of C_{61} remained in the reactor.	Air Products [34]

2.3 GAS-LIQUID MASS TRANSFER

In the absence of chemical reactions, the gas (A) diffuses into a liquid (B) and the mass transfer rate can be expressed using the following diffusivity Equation (2-3):

$$\frac{\partial c_A}{\partial t} = -D_{AB}\frac{\partial^2 c_A}{\partial x^2} \quad (2\text{-}3)$$

The steady-state mass transfer flux through the liquid film can be described according to the two-film theory by Equation (2-4).

$$J_i = k_{L,i}a(C_i^* - C_{i,L}) \quad (2\text{-}4)$$

Where C_i^* represents the solute concentration at the gas-liquid interface, $C_{i,L}$ is the solute concentration in the liquid bulk, k_L is the liquid-side mass transfer coefficient, and *a* represents the gas-liquid interfacial area. The following section will summarize the effect of various operating parameters on k_La and *C**.

2.4 LIQUID-SIDE VOLUMETRIC MASS TRANSFER COEFFICIENTS k_La IN AGITATED REACTORS

Physical and chemical methods were used to measure the gas-liquid interfacial area (*a*) and mass transfer coefficients (k_L) in multiphase systems. The gas-liquid interfacial area was measured using different physical and chemical methods. Physical methods, including photography, light reflection and light scattering were used, however, they were restricted to transparent contactors

having low gas holdup. Other physical methods, including γ–ray radiography and real time neutron radiography were also used to estimate *a*. While the aforementioned methods reveal the gas bubble contributions to *a*, other techniques were devised to determine the impact of gas-liquid interface ripple on *a*. For instance, Muenz and Marchello [48] measured the wave frequency using a stroboscope and determined the interface amplitude through analysis of the refractive surface properties via a photovolt photometer and densitometer. Moreover, Vazquez-Una et al. [49] used a CDD camera viewing the surface at a 45° angle to calculate through digitized image analysis the wavelength, λ. They determined the surface peak-to-peak amplitude and frequency from the surface displacement recorded using a vertically oriented laser triple-range distance-measuring device.

The chemical methods, on the other hand, were used to measure the gas-liquid interfacial area using a fast chemical reaction, where the reaction kinetics should be known in order to calculate *a*. Midoux and Charpentier [50] thoroughly reviewed various chemical reactions for measuring the gas-liquid interfacial area, *a*.

Physical and chemical methods were also used to measure the volumetric mass transfer coefficient (k_La) since it was found that the liquid-side mass transfer coefficient (k_L) strongly dependent on the turbulence induced in the multiphase systems. Among the physical methods is the transient physical gas absorption (TPGA) technique, which appears to be a simple and direct method for measuring k_La. For instance, Chang and Morsi [51] developed a powerful model to describe the transient pressure decline, based on a modified Peng-Robinson equation of state (EOS) and mass balance. In their method, the decline of the total pressure of the system with time was recorded, and in conjunction with total mole and volume balances, k_La values were obtained under high pressures and temperatures for numerous gases (CO, H_2, CH_4, CO_2, N_2, He,

etc.), into different liquids (hexane, toluene, cyclohexane, methanol, Silicone oil, molten wax, polyalphaolefins, etc.) in the absence and presence of solids (glass beads, alumina, Puralox, iron oxides, etc.). The improvement brought by this model was discussed elsewhere [52]. The chemical methods for measuring k_La we reviewed by Danckwerts et al. [53], Astarita [54] and Charpentier [55]. In these methods, a slow chemical reaction with known kinetics was employed to obtain k_La. The problems encountered in using these methods, however, were due to the difficulty in controlling temperature and the lack of reliable kinetics.

The liquid-side mass transfer coefficient (k_L) could be indirectly calculated, knowing both the gas liquid interfacial area (a) and the volumetric mass transfer coefficient (k_La) determined using any of the physical methods described above. However, one must measure k_La and a simultaneously, i.e., under the same hydrodynamics in order to calculate a meaningful value of k_L. This is because as mentioned above k_L strongly depends on the turbulence induced in the multiphase system. The liquid-side mass transfer coefficient (k_L) was also calculated using a chemical reaction with known kinetics and a contactor with known surface area (gas-liquid interface). The knowledge of the total absorption rate, equilibrium solubility, and reaction kinetics would enable the calculation of k_L [55]. Again, the difficulty in this method resides in the stability of the liquid film on the surface area of the contactor.

2.4.1 Factors Affecting the Volumetric Liquid-Side Mass Transfer Coefficient, k_La

The volumetric mass transfer coefficients are affected by numerous factors ranging from the physicochemical properties of the gas-liquid system (liquid nature, surface tension, viscosity and gas nature) to the operating conditions (pressure, temperature, mixing speed and solid

concentration) and reactor geometry. The following section summarizes the effects of operating conditions on k_La in gas inducing reactors (GIRs) as reported in the literature.

2.4.2 Effect of Pressure on k_La

The k_La values are strongly dependent on the gas-liquid system used and on the range of pressure investigated and were reported to increase [56-63], remain unaffected [64-69] or even decrease [70] with increasing pressure. A summary of these investigations is provided in Table 2-2. Most of these investigations related the effect of pressure on k_La to the variation of the physicochemical properties of the gas-liquid system due to the increased gas solubility, which decreases both surface tension and viscosity. Due to these conflicting impacts of viscosity and surface tension on k_La, the resultant impact may result in no effect, an increase or a decrease of k_La depending on the degree of change of the actual physical properties of the gas-liquid system.

2.4.3 Effect of Temperature on k_La

Similarly, k_La values were reported to increase [56, 58, 61, 63, 64, 66, 67, 69], have no or little effect [57] or decrease[58] with increasing temperature. A summary of these investigations is provided in Table 2-3. The change in k_La with temperature is mainly due to the effect of temperature on the liquid physicochemical properties. The liquid viscosity and surface tension decrease with increasing temperature, resulting in an decrease of the average bubble size and consequently an increase of the interfacial area, a. Moreover, increasing the temperature will also increase the diffusivity of the gas into the liquid and subsequently k_L since it is proportional to

the diffusivity to power 0.5 to 1.0. Such changes to a and k_L would ultimately lead to an increase, a decrease or no effect on k_La depending on the system nature and operating conditions used.

2.4.4 Effect of Mixing Speed on k_La

Increasing mixing speed has been reported to strongly increase the volumetric liquid-side mass transfer coefficients [56-65, 67, 69, 71-75], as shown Table 2-4. This behavior is due to the increased amount of induced gas into the liquid with increasing mixing speeds, which results in a higher gas holdup and interfacial area, a. Moreover, increasing the mixing speed increases the shear rate which, according the two film theory, decreases the liquid film thickness and subsequently k_L. However, a critical mixing speed, beyond which no increase in k_La is observed, has been reported by several investigators in small scale reactors [63, 71-73]. This behavior is due to the fact that the impeller reaches a maximum pumping capacity, and hence a maximum gas holdup, thus resulting in no further enhancement to k_La.

2.4.5 Effect of Liquid Nature on k_La

Karandikar et al. [58, 60, 61] and Chang et al.[62], reported a decrease in k_La with increasing the carbon number for hydrocarbons, such as alkanes (C_nH_{2n+2}). This effect can be related to the increase of viscosity of the n-alkane with increasing carbon number. Moreover, Albal et al. [65] reported that k_La increases with decreasing the viscosity and surface tension of the liquid. These effects on k_La are due to the increase of the gas diffusivity into the liquid with decreasing viscosity and also due to the decrease in the average bubble size with decreasing surface tension.

Table 2-2: Literature Survey on the Effect of Pressure on k_La

Gas	Liquid/Slurry	Reactor Type/ Operating Conditions	Results	Reference
H_2	2-propanol/o-cresol/ mixture (2/3 2-propanol+ 1/3 o-cresol)/ Pyrex beads ($40<d_p<300\mu m$)	Mode: GIR, TD 5 cm T = 303-393 K, N= 800-1500 rpm, P = 0-30 bar, Solids up to 5 vol%,	No effect	Hichri et al.[76]
N_2	Cyclohexane (C_6H_{12})	Mode: GIR, TD 13 cm T = 297-423 K, N = 480-1800 rpm, P = 1-10 bar	a, ε_G increase with P No effect after 10 atm	Sridhar et al. [77]
H_2/He/N_2/ CO_2/Ar	Ethanol/p-xylene/water	Mode: SAR, TD 5.6 cm T = 273 K, N = 150-1400 rpm P = 2-100 bar	No effect for H_2O and ethanol Increase P, decrease k_L for p-xylene	Teramoto et al.[78]
He/O_2	Glycerin/water+CMC/ glass beads (75-150μm)/ oil shale particles	Mode: SAR, TD 10.2 cm T = 295 K, N =400-1000 rpm, P = 13.8-96.5 bar, Solid up to 30 vol%	No effect	Albal et al. [79]
H_2/CO	Gulf wax, MW 380	Mode: SAR T = 348-523 K, N = 800-1000 rpm P = 10-35 bar,	No effect	Albal et al.[80]
N_2/O_2	Cyclohexane (C_6H_{12})	Mode: GIR/SAR T = 330-430 K, N = 400-1200 rpm P = 7-35 bar	k_La slightly increases with P	Tekie et al. [81]
H_2/CO/N_2/ CH_4/C_2H_4	Hexane mixture/ Iron oxide catalyst	Mode: SAR T = 298-373 K, N = 400-1200 rpm P = 2-25 bar	k_La increases with P for H_2/CO/N_2 No effect for CH_4/C_2H_4	Inga et al.[57]
H_2/CO	n-Octacosane (n-$C_{28}H_{58}$)/ iron-based catalyst	Mode: SAR, TV 0.3 L T = 523 K, N = 250-1750 rpm, P = 10-30 bar	No effect	Miller et al. [82]
H_2/CO	F-T light(C_6-C_{11})/ F-T medium (C_{12}-C_{21})/ F-T heavy($\geq C_{22}$)/solid: glass bed (125-177μm)	Mode: SAR, TV 2.0 L T = 373-523 K, N = 800-1100 rpm, P = 10-40 bar, Solid up to 30 wt.%	k_La increases with P	Deimling et al.[58]

Table 2-2 (continued).

Gas	Liquid/Slurry	Reactor Type/ Operating Conditions	Results	Reference
H_2/CO	F-T medium (C_{11}-C_{22}) MW 201.5	Mode: GIR, TV 4 L T = 423-498 K, N = 700-1200 rpm P = 10-40 bar	k_La increases with P k_La increases with P for CO and decrease for H_2	Karandikar et al. [37]
H_2/CO/ CH_4/CO_2	F-T heavy ($\geq C_{22}$) MW 368.5	Mode: GIR, TV 4 L T = 423-498 K, N = 700-1200 rpm, P = 10-40 bar,	k_La increases with P for $CO/H_2/CH_4/CO_2$ at 700 rpm, decreases for H_2/CO_2 at 1000-1200 rpm No effect for CO/CH_4	Karandikar et al. [83]
CO	n-hexane/n-decane/ n-tetradecane	Mode: GIR, TV 4 L T = 328-428 K, N = 800-1200 rpm, P = 1-50 bar,	k_La slightly increases with P	Chang et al. [84]
N_2	Water	Mode: GSR, TV 1.6 L T = 293 K, P = 1-100 bar	k_La decreases with P	Maalej et al.[70]

Table 2-3: Literature Survey on the Effect of Temperature on k_La

Gas	Liquid/Slurry	Reactor Type/ Operating Conditions	Results	Reference
H_2	2-propanol/o-cresol/ mixture (2/3 2-propanol+ 1/3 o-cresol)/ Pyrex beads ($40<d_p<300\mu m$)	Mode: GIR, TD 5 cm, T = 303-393 K, N = 800-1500 rpm, P = 0-30 bar, Solid up to 5 vol%	k_La increases with T	Hichri et al. [76]
N_2	Cyclohexane (C_6H_{12})	Mode: GSR, TD 13 cm, T = 297-423 K, N = 480-1800 rpm, P = 1-10 bar	Contradicting effects reported	Sridhar et al. [77]
N_2/H_2	Ethanol/water/ hydrogenation mixture/ Ni Raney particles (10-15μm)	Mode: GIR, TV 0.5 L, T = 293-353 K, P = 10-50 bar	k_La increases with T	Dietrich et al. [85]
H_2/CO	Gulf wax, MW 380	Mode: SAR T = 348-523 K, N = 800-1000 rpm, P = 10-35 bar	k_La increases with T	Albal et al.[80]
N_2/O_2	Cyclohexane (C_6H_{12})	Mode: GIR/SAR, T = 330-430 K, N = 400-1200 rpm P = 7-35 bar,	k_La increases with T	Tekie et al. [81]
$H_2/CO/N_2/CH_4/C_2H_4$	Hexane mixture/ Iron oxide catalyst	Mode: SAR, T = 298-373 K, N = 400-1200 rpm, P = 2-25 bar	Very small effect of temperature on k_La	Inga et al.[57]
H_2/CO	F-T light(C_6-C_{11})/ F-T medium (C_{12}-C_{21})/ F-T heavy($\geq C_{22}$)/solid: glass bed (125-177μm)	Mode: SAR, TV 2.0 L, T = 373-523 K, N = 800-1100 rpm, P = 10-40 bar, Solid up to 30 wt.%	k_La increases with T for F-T light & heavy k_La decreases with T for F-T medium	Deimling et al.[58]
H_2/CO	F-T medium (C_{11}-C_{22}) MW 201.5 +effect of water	Mode: GIR, TV 4 L, T = 423-498 K, N = 700-1200 rpm P = 10-40 bar,	k_La increases with T for F-T liquid saturated with water	Karandikar et al. [37]
O_2	water	Mode: GIR, TD 29 cm T = 293-313 K, N = 900-1300 rpm, P = 1-1.2 bar,	k_La increases with T	Chen et al. [69]

Table 2-4: Literature Survey on the Effect of Mixing Speed on k_la

Gas	Liquid/Slurry	Reactor Type/ Operating Conditions	Results	Reference
CO	n-hexane/n-decane/ n-tetradecane	Mode: GIR, TV 4 L, T = 328-428 K, N = 800-1200 rpm, P = 1-50 bar	k_La increases with N	Chang et al. [84]
O_3	Water	Mode: GIR, Ambient conditions (298 K, 1 bar) N = 500-1600 rpm	k_La increases with N Levels off at 1400 rpm	Hsu et al.[86]
H_2	2-propanol/o-cresol/ mixture (2/3 2-propanol+ 1/3 o-cresol)/ Pyrex beads ($40<d_p<300\mu m$)	Mode: GIR, TD 5 cm, T = 303-393 K, N = 800-1500 rpm, P = 0-30 bar, Solid up to 5 vol%	k_La increases with N	Hichri et al.[76]
N_2	Cyclohexane	Mode: GSR, TD 13 cm, T = 297-423 K, N = 480-1800 rpm, P = 1-10 bar	k_La increases with N, levels off at high N	Sridhar et al. [77]
He/O_2	Glycerin/water+CMC/ glass beads (75-150μm)/ oil shale particles	Mode: SAR, TD 10.2 cm, T = 295 K, N = 400-1000 rpm, P = 13.8-96.5 bar, Solid up to 30 vol%	k_La increases with N	Albal et al. [79]
N_2/H_2	Ethanol/water/ hydrogenation mixture/ Ni Raney particles (10-15μm)	Mode: GIR, TV 0.5 L, T = 293-353 K, P = 10-50 bar	k_La increases with N	Dietrich et al.[85]
N_2/O_2	Cyclohexane	Mode: GIR/SAR T = 330-430 K, N = 400-1200 rpm P = 7-35 bar,	k_La increases with N	Tekie et al. [81]
$H_2/CO/N_2/CH_4/C_2H_4$	Hexane mixture/ Iron oxide catalyst	Mode: SAR, T = 298-373 K, N = 400-1200 rpm, P = 2-25 bar,	k_La increases with N	Inga et al.[57]
$H_2/CO/N_2/CO_2$	Vestowax SH105	Mode: SAR, TV 1 L, T = 453-553 K, P = 1-60 bar	k_La increases with N	Ledakowicz et al.[87]
H_2/CO	n-Octene/ethanol/water	Mode: GIR, TV 0.6L, T = 323K, N =1100-2500 rpm, P = 10-150 bar,	k_La increases with N	Lekhal et al. [88]

Table 2-4 (continued).

Gas	Liquid/Slurry	Reactor Type/ Operating Conditions	Results	Reference
H_2/CO	F-T medium (C_{11}-C_{22}) M.W. 201.5 +effect of water	Mode: GIR, TV 4L, T = 423-498K, N = 700-1200 rpm, P = 10-40 bar	k_La increases with N Effect of	Karandikar et al. [37]
H_2/CO/ CH_4/CO_2	F-T heavy ($\geq C_{22}$) M.W. 368.5 + effect of water	Mode: GIR, TV 4L, T = 423-498K, N = 700-1200 rpm, P = 10-40 bar,	k_La increases with N	Karandikar et al.[83]
H_2/CO	F-T light(C_6-C_{11})/ F-T medium (C_{12}-C_{21})/ F-T heavy($\geq C_{22}$)/solid: glass bed (125-177μm)	Mode: SAR, TV 2.0L, T = 373-523K, N = 800-1100 rpm, P =10-40 bar, Solid up to 30 wt.%	k_La increases with N	Deimling et al.[58]
O_3	Water	Mode: GIR, TD 29 cm, T = 290-303 K, N = 600-1300 rpm	k_La increases with N, levels off above 1000 rpm	Hsu et al.[71]
O_2	water	Mode: GIR, TD 29 cm, T = 293-313 K, N = 900-1300 rpm, P = 1-1.2 bar,	k_La increases with N	Chen et al.[69]
H_2/CO	F-T medium (C_{11}-C_{22}) M.W. 201.5 +effect of water	Mode: GIR, TV 4L, T = 423-498K, N = 700-1200 rpm, P = 10-40 bar	k_La increases with N	Karandikar et al. [37]
H_2/CO/ CH_4/CO_2	F-T heavy ($\geq C_{22}$) MW 368.5 + effect of water	Mode: GIR, TV 4L, T = 423-498K, N = 700-1200 rpm, P = 10-40 bar	k_La increases with N	Karandikar et al.[83]
H_2/CO	F-T light(C_6-C_{11})/ F-T medium (C_{12}-C_{21})/ F-T heavy($\geq C_{22}$)/solid: glass bed (125-177μm)	Mode: SAR, TV 2.0L, T = 373-523K, N = 800-1100 rpm, P = 10-40 bar, Solid up to 30 wt.%	k_La increases with N	Deimling et al.[58]
O_3	Water	Mode: GIR, TD 29 cm, T = 290-303 K, N = 600-1300 rpm	k_La increases with N levels off above 1000 rpm	Hsu et al.[71]
O_2	Water	Mode: GIR, TD 29 cm T = 293-313 K, N = 900-1300 rpm, P = 1-1.2 bar	k_La increases with N	Chen et al.[69]

2.4.6 Factors Affecting the Solubility *C**

As can be seen in Equation (2-4), the equilibrium solubility, C^* is a parameter of prime importance for determining the rate of mass transfer in gas-liquid processes. Table 2-5 presents a literature survey of the solubility of gases in organic or paraffinic liquids under high pressures and temperatures. As can be observed in this table, for most of these gas- liquid systems, the solubility appeared to increase linearly with pressure and therefore follows Henry's law within the pressures investigated. The C^* of gases in organic liquids was also reported to decrease with increasing molecular weight (carbon number) of organic liquid in homologous hydrocarbon series [62, 89]. Depending on the gas-liquid system considered as well as the temperature range studied, C^* values can either decrease or increase with increasing temperature. For instance, the solubilities for Ar, H_2, N_2, He and CO in n-paraffins were reported to increase with increasing temperature [66, 90-97], whereas those for CO_2, CH_4, C_2H_6, C_2H_4, and C_3H_8 were reported to decrease [89, 90, 95, 96]. Several investigators [63, 95, 96, 98-101] measured the solubility of different gases in the different organic liquids (mostly in n-paraffins) and reported the following order for the solubility values:

$$C^*_{He} < C^*_{H_2} < C^*_{N_2} < C^*_{CO} < C^*_{CH_4} < C^*_{CO_2} < C^*_{C_2H_4} < C^*_{C_2H_6} < C^*_{C_3H_8}$$

Table 2-5: Literature Survey on Solubilities of Gases in Hydrocarbon Liquids/Silicone Oil

Gases	Solvent	MW	T (K)	P (bar)	System	Reference
$H_2/CO/CH_4/CO_2/C_2H_6/C_2H_4$	Sasol wax (n-$C_{43}H_{88}$)	605	473-573	10-50	Diffusion cell (Shaking mech.)	Chou et al.[102]
H_2/CO	Gulf wax	380	348-523	10-35	Stirred reactor (SAR)	Albal et al.[80]
$H_2/CO/CO_2/Ar/CH_4/C_2H_6/C_2H_4/C_3H_8/C_4H_{10}$	Sasol Wax	464±53	433-513	3-11	Diffusion cell (Shaking mech.)	Van Vuuren et al.[103]
$CH_4/C_2H_6/CO_2$	Mobil wax (n-$C_{61}H_{124}$)	857	473-573	10-50	Equilibration cell	Tsai et al.[89]
CO/H_2	n-C_{20}/C_{28}/C_{36}/ Mobil F-T wax	282-857	373-573	10-50	Equilibration cell	Huang et al.[97]
$CO/H_2/CO_2/CH_4/C_2H_6/C_2H_4$	n-C_{20}/C_{28}/C_{30}/C_{43}/C_{61}/C_{95}/ Sasol wax Mobil F-T wax	282-1332	-	-	Lacombe-Sanchez EOS Correlation (for heavy n-paraffin)	Chou et al.[98]
$H_2/N_2/CO$	n-C_{12}	170	344-410	7-132	Rocking cell	Gao et al.[104]
$CO/H_2/CH_4/CO_2$	F-T heavy fraction	368	423-498	7-45	Stirred reactor (GIR)	Karandikar et al.[83]
CO/H_2	F-T medium fraction (C_{11}-C_{20})	201	423-498	10-40	Stirred reactor (GIR)	Karandikar et al.[37]
$H_2/CO/CH_4/CO_2/C_2H_6/C_2H_4$	Light & heavy n-paraffins n-$C_{20}H_{42}$/n-$C_{28}H_{58}$/n-$C_{36}H_{74}$ Sasol wax ($C_{43}H_{88}$) Mobil wax ($C_{61}H_{124}$)	282-506	-	-	Correlation based on fluctuation solution theory	Campanella [100]
H_2/CO	n-$C_{20}H_{42}$/n-$C_{28}H_{58}$/ n-$C_{61}H_{124}$	282-857	373-573	10-50	Equilibration cell	Huang et al.[105]
CO	n-C_6H_{14}/n-$C_{10}H_{22}$/n-$C_{14}H_{30}$	86-198	328-428	1-50	Stirred reactor (GIR)	Chang et al. [84]
$H_2/CO/CO_2$	n-paraffins C_{20}-C_{44}	282-618	-	-	Correlation using a lattice-gas model	Campanella [106]

Table 2-5 (continued).

Gases	Solvent	MW	T (K)	P (bar)	System	Reference
$H_2/CO/N_2/CH_4/C_2H_4$	Hexane mixture: 2 methyl pentane (6.73%)/ 3 methyl pentane (14.17%)/ Hexane (64.55%)/ Methylcylopentane (14.55%)	85.88	398-303	5-25	Stirred reactor (SAR)	Inga [107]
N_2/O_2	Cyclohexane	78	330-430	7-35	Stirred reactor	Tekie et al. [81]
$CH_4/C_2H_6/CO/H_2$	n-Alkanes (up to C_{16})/ 1-alkenes (C_2 to C_{16})	28-226	-	-	Statistical Associating Fluid Theory EOS	Ghosh et al. [108]
H_2	Cyclohexane/Gas oil	78	298-675	Up to 40	Stirred reactor (GIR)	Ronze et al. [91]
$H_2/CO/CO_2/H_2O$/n-C_2H_6 to C_6H_{14}/ CH_3OH/C_2H_5OH/ 1-C_3H_7OH/ 1-C_4H_9OH/ 1-$C_5H_{11}OH$/ 1-$C_6H_{13}OH$	Tetraethyleneglycol ($C_8H_{18}O_5$)/n-$C_{16}H_{34}$/ n-$C_{28}H_{58}$/1-$C_{16}H_{33}OH$/ phenanthrene ($C_{14}H_{10}$)/	178-394	293-553	0.6-55	Stirred reactor (SAR)	Breman et al. [109]
H_2	2-propanol/o-cresol	60-108	303-393	0-30	Stirred reactor (GIR)	Hichri et al. [76]
$H_2/CO/N_2/CH_4$	Isopar-M (C_{10}-C_{16})/ hexane mixture	85.88-192	298	1.7-8	SBCR	Behkish et al. [110]
N_2	n-$C_{10}H_{22}$/n-$C_{20}H_{42}$/ n-$C_{28}H_{58}$/n-$C_{36}H_{74}$	142-506	323-423	Up to 180	Equilibrium cell	Tong et al. [111]
H_2/CO	n-$C_{28}H_{58}$	394	528	10-30	Stirred reactor (SAR)	Miller et al. [82]
CO/H_2	F-T heavy/medium/light	114-368	373-523	10-40	Stirred reactor (SAR)	Deimling et al.[38]

3.0 OBJECTIVES

The objectives of this work are: (1) to statistically measure the solubilities and volumetric liquid-side mass transfer coefficients of two gases, He and N_2, in addition to their mixtures in two liquids, SpectraSyn Polyalphaolefin and Silicone Oil, which could be used as startup liquid in F-T synthesis, in a wide range of operating conditions; (2) to investigate the effects of operating variables as well as the gas and liquid natures on the solubility and the volumetric liquid-side mass transfer coefficients; and (3) to explore the feasibility of using different liquid including those used in this study as potential startup liquids for F-T synthesis in SBCRs.

4.0 EXPERIMENTAL

4.1 OPERATING CONDITIONS USED

The equilibrium solubilities and volumetric mass transfer coefficients were measured under the operating conditions given in Table 4-1. A test matrix covering these conditions was devised following the Central Composite Statistical Design (CCSD) and analysis technique [112], which has been extensively used in our laboratory [113-116]. Repeat runs were also carried out in order to ensure the reproducibility of the experimental data. The distribution of experiments for 4 variables at 5 levels according to this CCSD is shown in Figure 4-1.

Table 4-1: Operating Conditions used in this Study

Reactor operating mode	Gas-Inducing Reactor (GIR)
He/N_2 Mixture	0% He/100% N_2, 25% He /75% N_2, 50% He /50% N_2, 75% He/ 25% N_2, 100% He/0% N_2
Liquid	Silicone Oil (DC-200, 100 cSt), SpectraSyn Polyalphaolefin
Pressure	4 - 30 bars
Temperature	298 - 398 K
Mixing speed	1000 - 1400 rpm

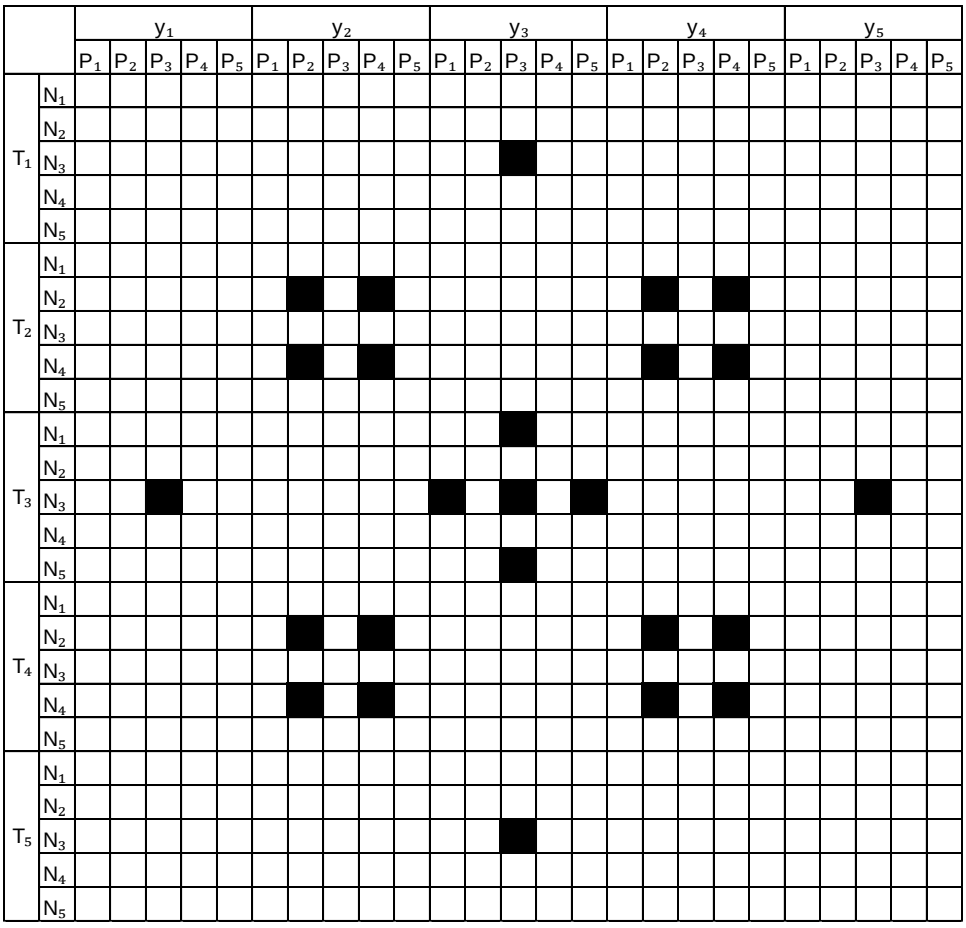

Figure 4-1: CCSD Approach for Experimental Distribution and Spatial Settings

4.2 GAS-LIQUID SYSTEM USED

4.2.1 Properties of the Gases Used

The gases used were He and N_2 as surrogates of H_2 and CO, respectively. The N2 and He were purchased from Valley National Gases (USA), with purities of 99.99% and 99.98%, respectively. The basic thermodynamics properties of these gases are given in the Table 4-2.

Table 4-2: Thermodynamic Properties of the Gases

Gases	MW (kg/kmol)	T_b (K)	T_C (K)	P_C (bar)	V_C (m^3/kmol)	Z_C	ω
N_2	28.013	77.35	126.10	33.94	0.0901	0.292	0.040
He	4.003	4.22	5.20	2.28	0.0573	0.302	-0.390
H_2	2.016	20.39	33.18	13.13	0.0642	0.305	-0.220
CO	28.010	81.70	132.92	34.99	0.0931	0.295	0.066

4.2.2 Properties of the Liquids Used

The two liquids investigated in this study were Silicone Oil DC-200 and SpectraSyn Polyalphaolefin. Silicone oil is composed of a linear chain of siloxane repeating units (-Si-O) and a variety of side chains (radical side groups). The molecular weight of Silicone Oil DC-200 is 236.53 kg/kmol and its molecular structure is shown in Figure 4-2. The SpectraSyn Polyalphaolefin is a mixture of hexadecane, octacosane and tetratetracontane with the composition given in Table **4-3** and molecular weight of 606.14 kg/kmol. It should be noted that Silicone has been reported to degrade between 130 and 180 ^oC (403 to 453 K) [117] where depolymerization of the polysiloane backbone occurs leading to the formation of cyclosiloxanes [118]. This was in agreement with our observations at temperatures greater than 140 oC, the color and viscosity of Silicone Oil changed.

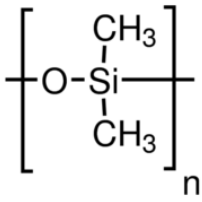

Figure 4-2: Molecular Structures of Silicone Oil DC-200 [119]

Table 4-3: Composition of SpectraSyn Polyalphaolefin [120]

Component	Formula	Mole %	Mass %
Hexadecane	$C_{16}H_{34}$	0.089	0.034
Octacosane	$C_{28}H_{58}$	14.000	9.395
Tetratetracontane	$C_{44}H_{90}$	85.910	90.570

4.2.3 Densities of the Liquid Used

The densities of Silicone Oil and SpectraSyn polyalphaolefin were measured inside a 200 ml graduated cylinder by recording the change in liquid volume with temperature over the range from 300 to 400 K. The experimental data are illustrated in Figures 4-3 and 4-4. The data were also correlated as a function of temperature by Equations (4-1) and (4-2).

$$\rho_{SiliconeOil}\ (kg/m^3) = 1185.3 - 0.7625T \quad (4\text{-}1)$$

$$\rho_{SpectraSyn}\ (kg/m^3) = 975.88 - 0.6T \quad (4\text{-}2)$$

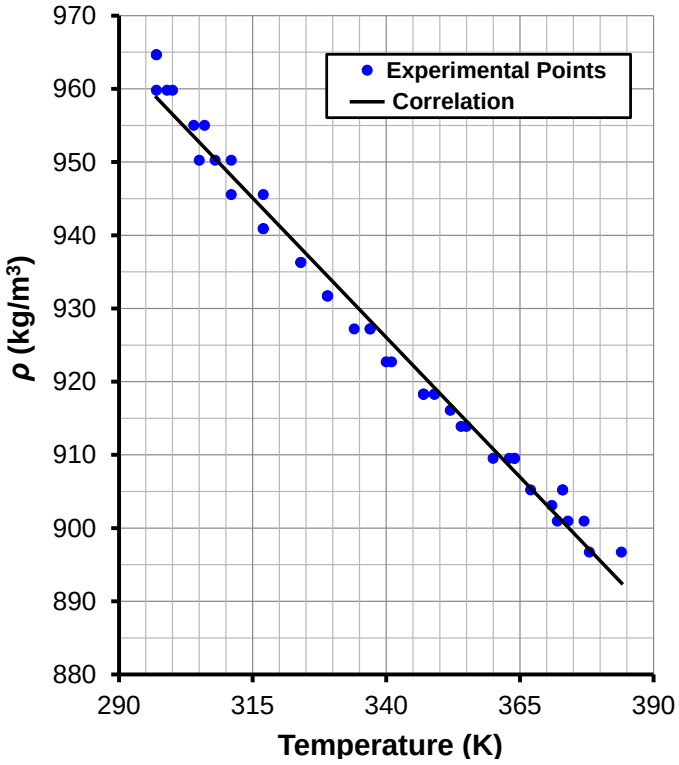

Figure 4-3: Effect of Temperature on the Density of Silicone Oil

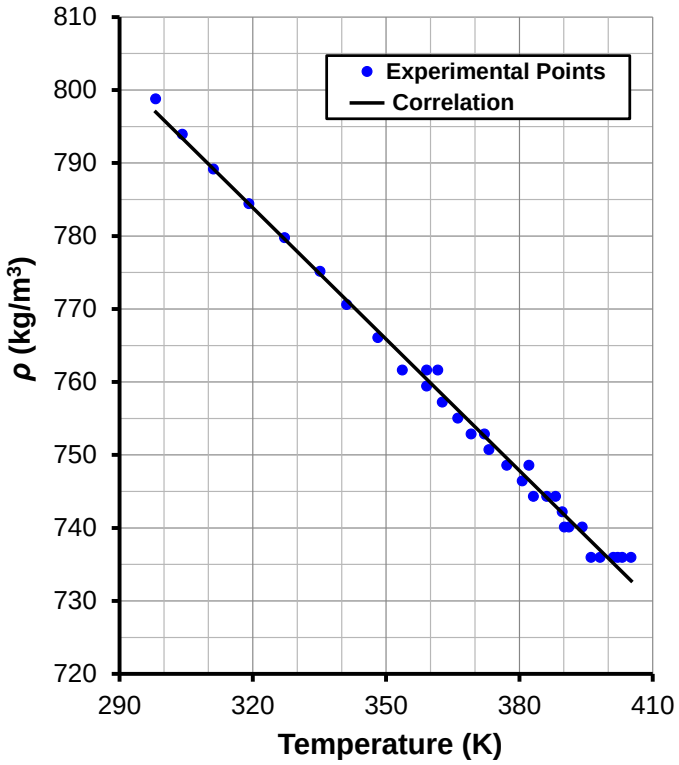

Figure 4-4: Effect of Temperature on the Density of SpectraSyn Polyalphaolefin

4.2.4 Viscosities of the Liquids Used

The viscosities of Silicone and SpectraSyn Polyalphaolefin were measured using a Cannon-Fenske viscometer over the temperature range from 300 to 450 K. The experimental data are shown in Figures 4-5 and 4-6. The data were also correlated as a function of temperature by Equations (4-3) and (4-4).

$$\mu_{SiliconeOil}\ (Pa \cdot s) = 20.028 \times 10^{-2} exp\left(\frac{1840}{T}\right) \quad (4\text{-}3)$$

$$\mu_{SpectraSyn}(Pa \cdot s) = 20.137 \times 10^{-4} exp\left(\frac{32026}{T}\right) \quad (4\text{-}4)$$

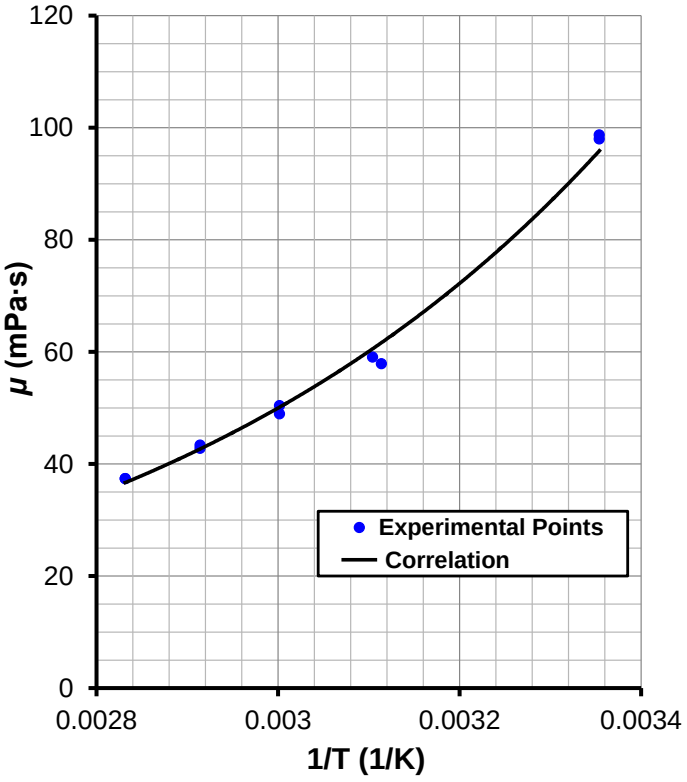

Figure 4-5: Effect of Temperature on the Viscosity of Silicone Oil

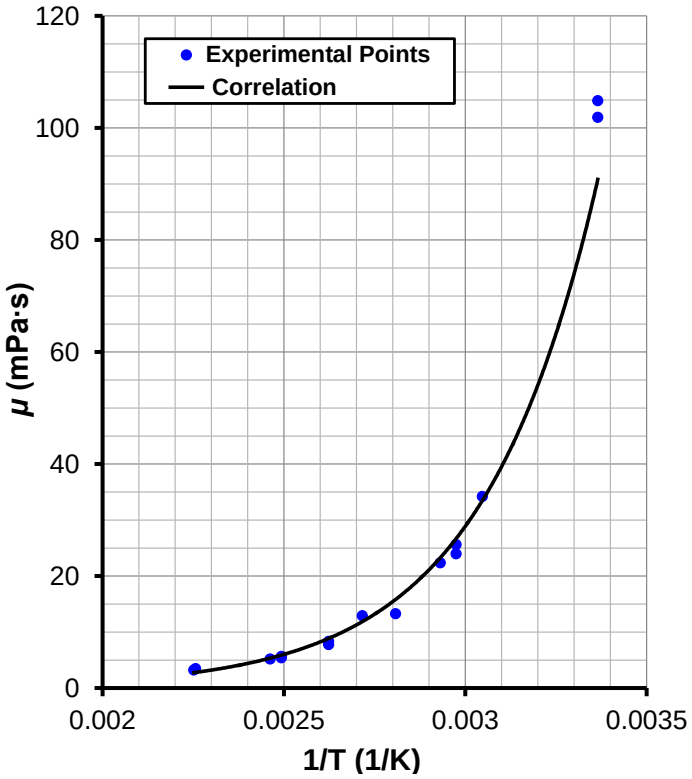

Figure 4-6: Effect of Temperature on the Viscosity of SpectraSyn Polyalphaolefin

4.2.5 Vapor Pressures of the Liquids Used

The vapor pressure of Silicone Oil was measured in a one-liter agitated Autoclave. The reactor was charged with 500 ml of Silicone Oil, vacuumed and heated to 420 K. The pressure was recorded every 5 minutes during both heating and cooling of the liquid. The vapor pressure of SpectraSyn Polyalphaolefin was predicted using the method developed by Marano and Holder [121-123]. The experimental data and the method predictions are shown in Figures 4-7 and 4-8, respectively. The experimental data of the Silicone Oil and the correlation predictions of the SpectraSyn Polyalphaolefin were also correlated as a function of temperature by Equations (4-5) and (4-6).

$$P^{v}_{SiliconeOil}\ (bar) = (8.208 \times 10^{-4})T - 0.2431 \quad (4\text{-}5)$$

$$P^{v}_{SpectraSyn}\ (bar) = (7.747 \times 10^{-14})exp(0.0505T) \quad (4\text{-}6)$$

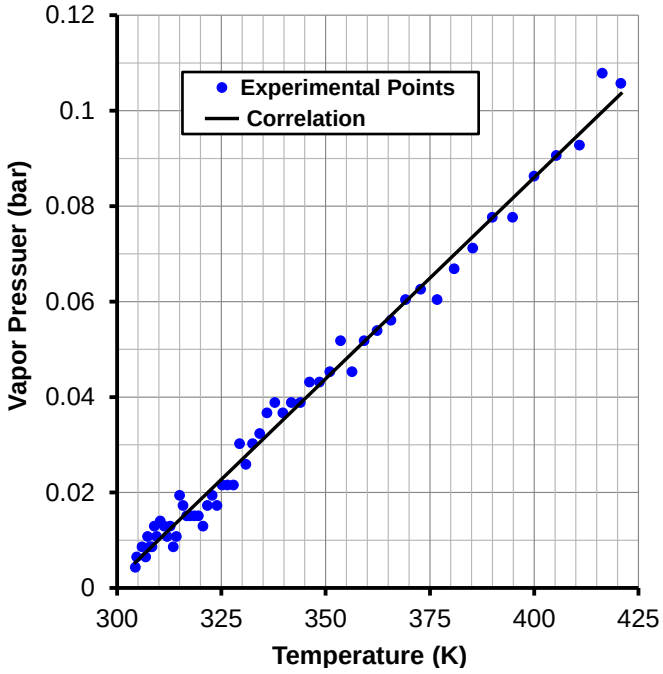

Figure 4-7: Effect of Temperature on the Vapor Pressure of Silicone Oil

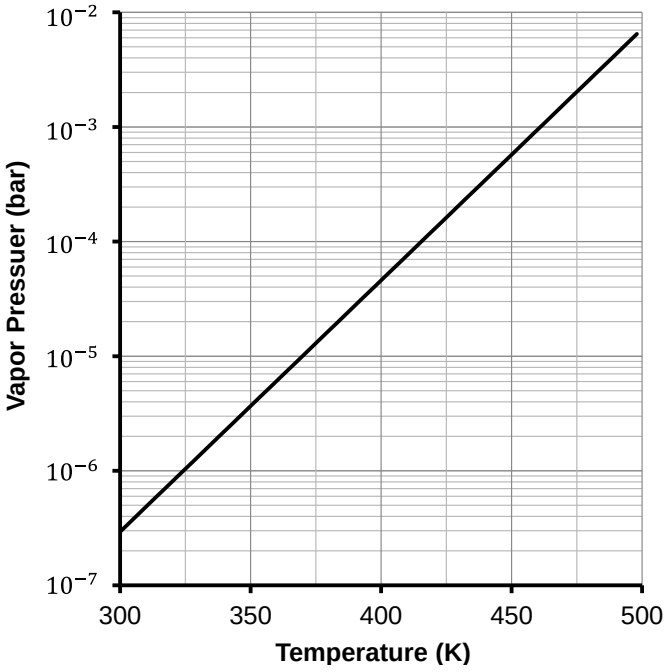

Figure 4-8: Effect of Temperature on the Vapor Pressure of SpectraSyn Polyalphaolefin
(Predictions using Marano and Holder [121-123])

4.2.6 Surface Tensions of the Liquids Used

The surface tension of Silicone Oil was correlated using the experimental data of Ricci et al. [124]. The surface tension of SpectraSyn Polyalphaolefin was predicted using the method developed by Marano and Holder [121-123]. The effect of temperature on the surface tensions for both liquids is shown in Figures 4-9 and 4-10, and the data as well as the predictions were correlated as a function of temperature by Equations (4-7) and (4-8).

$$\sigma_{Silicone\ Oil} = 0.0202 \ln\left(\frac{1}{T}\right) + 0.134 \quad (4\text{-}7)$$

$$\sigma_{SpectraSyn} = 0.033 \ln\left(\frac{1}{T}\right) + 0.218 \quad (4\text{-}8)$$

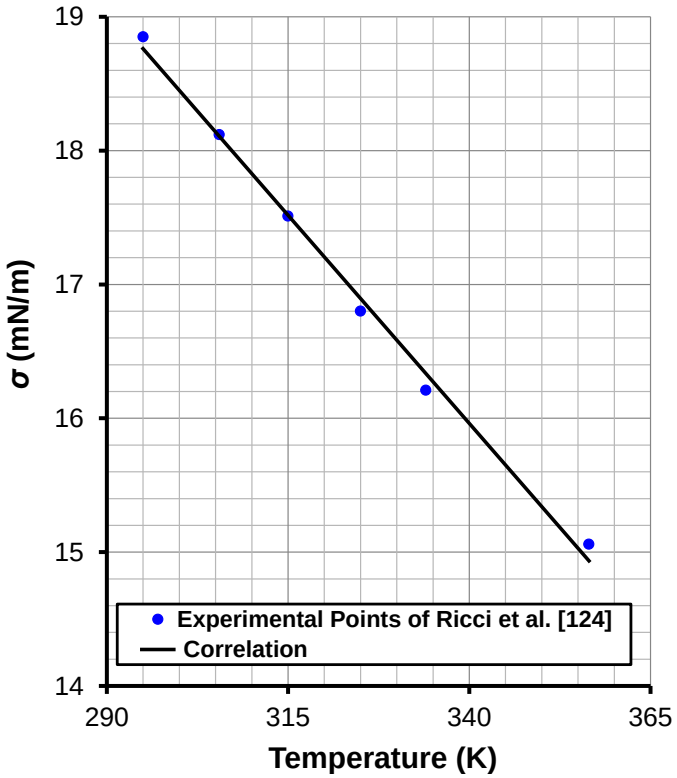

Figure 4-9: Effect of Temperature on the Surface Tension of Silicone Oil (Data from reference [124])

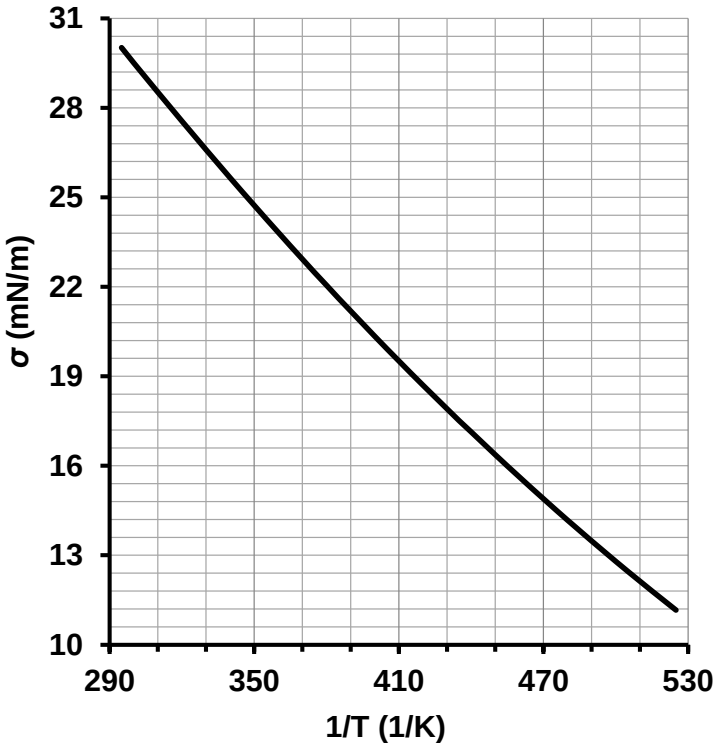

Figure 4-10: Effect of Temperature on the Surface Tension of SpectraSyn Polyalphaolefin
(Predictions using Marano and Holder [121-123])

4.2.7 Gases diffusivities in the Liquids Used

The diffusivities of the two gases used (N_2 and He) in the addition to the diffusivities of their surrogate H_2 and CO in the Silicone Oil and SpectraSyn Polyalphaolefin were calculated using the Wilke and Chang [125] equation:

$$D_{AB} = 0.1728 \times 10^{-16} \frac{(\lambda Mw_B)^{0.5} T}{\mu_L \upsilon_A^{0.6}} \qquad (4\text{-}9)$$

The subscripts *A* and *B* represent the gas and liquid components, respectively; λ is the association factor of the liquid-phase (λ = 1); and υ_A is the gas molar volume. Figures 4-11 and 4-12 show the diffusivities of He, N_2, CO and H_2 in the Silicone Oil and SpectraSyn Polyalphaolefin as a function of temperature, respectively.

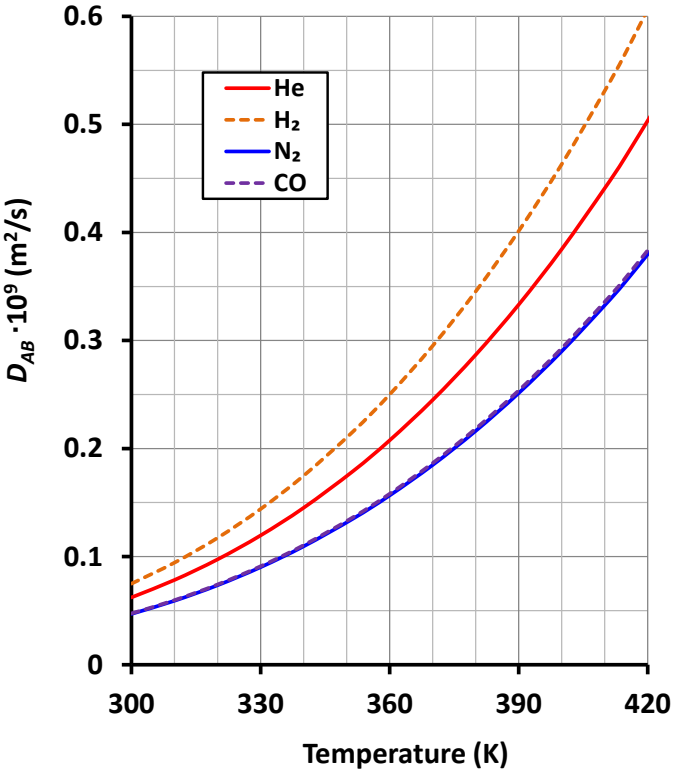

Figure 4-11: Diffusivities of Gases in Silicone Oil

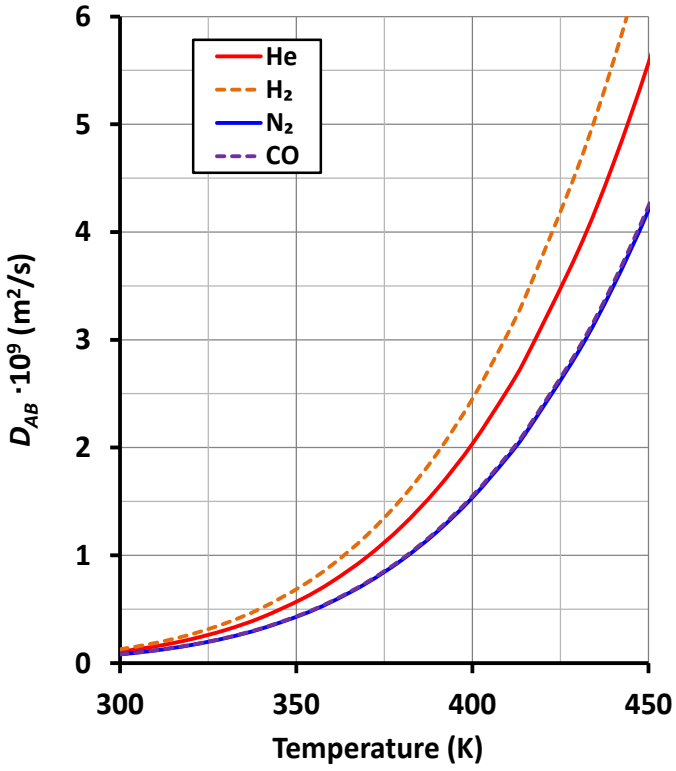

Figure 4-12: Diffusivities of Gases in SpectraSyn Polyalphaolefin

4.3 EXPERIMENTAL SETUP

4.3.1. One-Gallon Agitated ZipperClave Reactor

The experimental setup used is shown schematically in Figure 4-13. A photo of the setup is also shown in Figure 4-14. The experimental setup is composed of four parts: reactor, preheater, vacuum system and data acquisition system. The reactor is a 4-liter ZipperClave with an effective volume of 3.86 liters which can be used in three different modes of operation: Surface Aeration Reactor (SAR), Gas Inducing Reactor (GIR) and Gas Sparging Reactor (GSR). In these experiments, the reactor was operated in the GIR mode as shown in Figure 4-15.

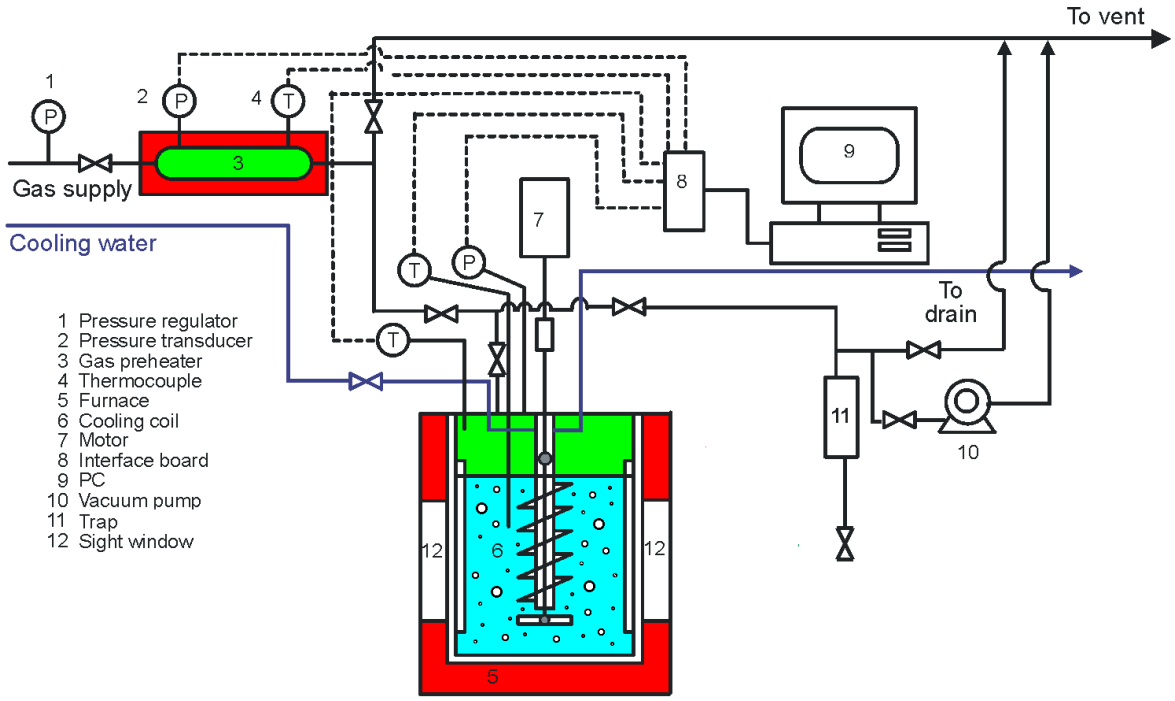

Figure 4-13: Schematic of the Experimental Setup of the 1-Gallon ZipperClave Reactor

Figure 4-14: 1-Gallon ZipperClave Reactor Equipment

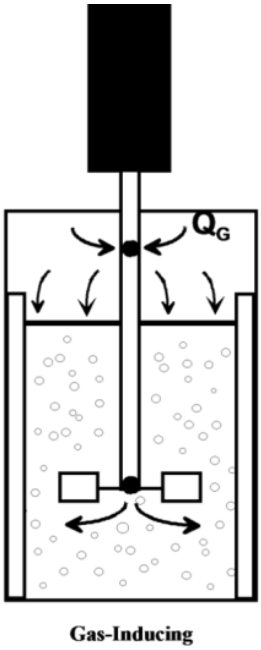

Figure 4-15: Gas Inducing Mode Operations inside the 1-Gallon ZipperClave Reactor

4.3.2. One-Liter Agitated Autoclave

A one-liter agitated Autoclaves was also used in order to measure the vapor pressure of Silicone Oil. The reactor is manufactured by Autoclave Engineers, Inc., and its details are given in Table 4-4.

Table 4-4: One-Liter Autoclave Reactor Features

Effective volume	1.028 liters
Maximum working pressure	5450 Psi
Maximum temperature	727.5 K
Baffles	Four baffles located symmetrically to prevent vortex formation
Impeller	6 flat-blade, connected to hollow shaft with four, 2.4 mm diameter holes

The reactor is also equipped with an internal cooling coil, an external heating jacket and thermal insulation. The agitators are driven by a magnetic drive to avoid any eccentricity. The pressure transducers and thermocouples were used to measure the change of pressure and temperature in both liquid and gas phases. The reactor was vacuumed to a minimum absolute pressure of 5 mm Hg, using a HYVAC-14, 2-stage mechanical vacuum pump. A liquid trap is located between the reactor and the pump to prevent any liquid from entering into the vacuum system and to monitor any possible liquid loss. The outlet of the vacuum pump is directly connected to a vent.

The vapor pressure data were recorded using a data acquisition module cDAQ-9172 by National Instruments. The module is connected to the thermocouples and pressure transducers with NI Bus 9211 and 9215, which are subsequently connected to a PC. The LabView software is used to monitor and record the pressures and temperatures during experiments.

4.4 EXPERIMENTAL PROCEDURES

The multi-step physical gas absorption method was followed to determine C* and k_La for He, N_2, and He/N_2 mixtures in the two liquids (Silicone Oil and SpectraSyn Polyalphaolefin).

The experimental procedure is given below:

1. The reactor is charged with a known amount of liquid.
2. The reactor is closed and vacuumed.
3. The gas is charged from the gas cylinders into the preheater.
4. The gases in the reactor and the preheater are heated to the desired temperature.
5. The gas is charged from the preheater to the reactor up to the desired pressure without any mixing.
6. The pressure and temperature in the reactor and preheater are recorded while the liquid in the reactor is agitated at a given mixing speed until the pressure becomes constant and the thermodynamic equilibrium is reached. After equilibrium, the mixing and recording of data are stopped.
7. The values of pressure and temperature in both reactor and preheater are recorded as functions of time.
8. Steps 5 through 7 were repeated in order to accumulate data points at various pressures as illustrated in Figure 4-16.

This procedure was repeated at every run with different temperatures, mixing speeds and gas compositions. After each run, C^* and k_La values were calculated.

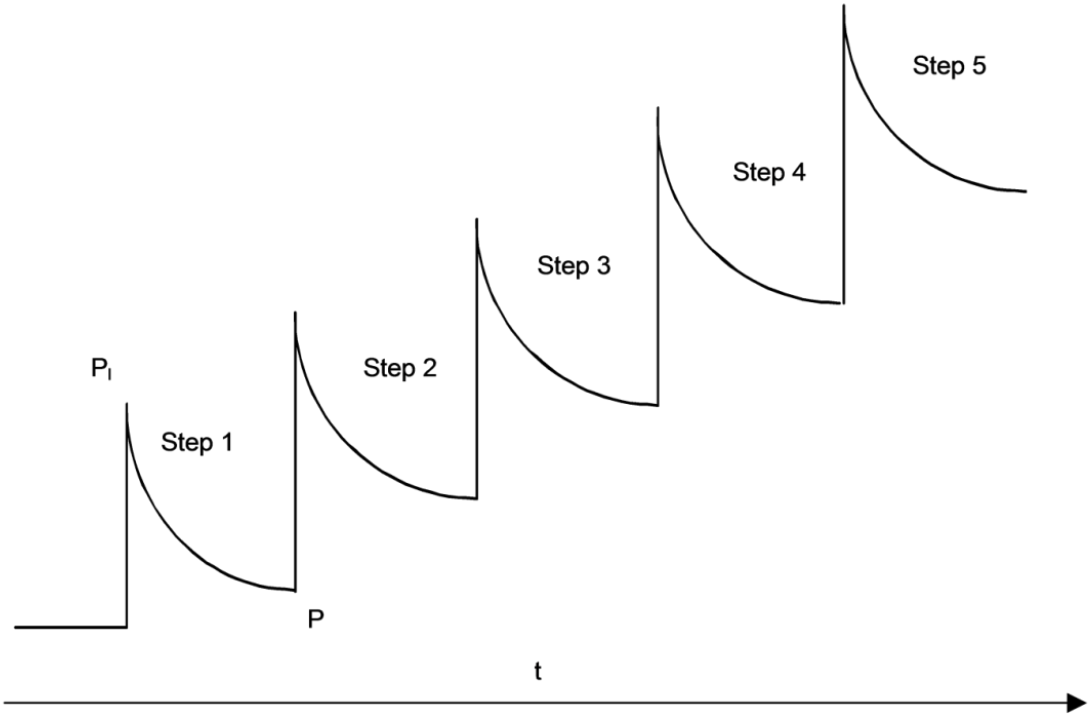

Figure 4-16: Multi-Step Procedure Technique

5.0 CALCULATIONS

The calculation methods for the determination of C^* and k_La for He, N_2 and their mixtures in Silicone Oil and SpectraSyn Polyalphaolefin are presented in the following section.

5.1 EQUILIBRIUM SOLUBILITY (C*) CALCULATIONS

The equilibrium solubility (C^*) was determined from the steady-state portion of the pressure decline (P vs t) curve. The Peng-Robinson Equation of State (PR-EOS), coupled with mass balances around both the preheater and reactor were used for the calculations.

5.1.1 Peng-Robinson Equation of State

The Peng Robinson Equation of state (PR-EOS) was used to determine the number of moles of gas charged from the preheater to the reactor in addition to the number of moles remaining in the gaseous phase of the reactor after absorption was complete. Equation (5-1) is the general form of the PR-EOS.

$$P = \frac{RT}{v-b} - \frac{a(T)}{v(v+b)+b(v-b)} \qquad (5\text{-}1)$$

Equation (5-1) can also be expressed in terms of the compressibility factor Z, as in Equation (5-2). Since Equation (5-2), is a cubic equation, it would result in three real roots. For a single-phase system, one real root and two imaginary roots are obtained.

$$Z^3 - (1 - B) \cdot Z^2 + (A - 3B^2 - 2B) \cdot Z - (AB - B^2 - B^3) = 0 \quad (5\text{-}2)$$

Where:

$$A = \frac{aP}{R^2T^2} \quad (5\text{-}3)$$

$$B = \frac{bP}{RT} \quad (5\text{-}4)$$

The coefficients in Equations (5-3) and (5-4) are:

$$a = \sum_i \sum_j y_i y_j a_{ij} \quad (5\text{-}5)$$

$$a = \sum_i y_i b_i \quad (5\text{-}6)$$

$$a_{ij} = \left(1 - \delta_{ij}\right) a_i^{1/2} a_j^{1/2} \quad (5\text{-}7)$$

$$a_i = 0.45724 \frac{R^2 T_c^2}{P_c^2} \left[1 + \kappa\left(1 - T_R^{1/2}\right)\right]^2 \quad (5\text{-}8)$$

$$a_i = 0.0778 \frac{R^2 T_c}{P_c} \quad (5\text{-}9)$$

$$\kappa = 0.37464 + 1.5244\omega - 0.26992\omega^2 \quad (5\text{-}10)$$

Equation (5-2) was used to calculate the number of moles before and after absorption in the gas-phase in order to calculate the gas solubility.

5.1.2 Equilibrium Solubility, C*

In order to calculate *C**, the following assumptions were made: (1) the gas in both the reactor and the preheater were assumed to be non-ideal, and therefore the Peng-Robinson EOS was used; (2) the gas and liquid are well mixed and uniform; (3) no gas is absorbed before mixing; and (4) the liquid volume is not affected by the amount of gas absorbed. The equilibrium solubility (*C**) is calculated using Equation (5-11), which represents the difference in the number of moles of gaseous species absorbed into the liquid at equilibrium, by knowing the change in the number of moles of the gas-phase in the reactor.

$$C_i^* = \frac{N_{i,I} - N_{i,F}}{V_L} \tag{5-11}$$

Where $N_{i,I}$ is the initial number of moles of species (*i*) in the gas-phase inside the reactor prior absorption; and $N_{i,F}$ is the final number of moles of species (*i*) remaining in the gas-phase inside the reactor at thermodynamic equilibrium.

$N_{i,I}$ and $N_{i,F}$ are calculated as follows:

$$N_{i,I} = \frac{V_G}{RZ_{i,I}T_I}\left(P_{i,I} - P^v\right) \tag{5-12}$$

$$N_{i,F} = \frac{V_G}{RZ_{i,F}T_{F,avg}}\left(P_{Fi,I} - P^v\right) \tag{5-13}$$

Where T_I is the initial temperature before absorption and $T_{F,avg}$ is the average temperature of the gas-phase during the absorption. The volume of the gas phase (V_G) is determined from the difference between the reactor overall volume and the liquid-phase volume inside the reactor by Equation (5-14).

$$V_G = V_{reactor} - \left(\frac{m_{liquid}}{\rho_{liquid}}\right) \quad (5\text{-}14)$$

Where, ρ_{liquid} and m_{liquid} represent the density and mass of the liquid-phase, respectively. The solubility, C* is subsequently calculated by substituting Equations (5-12), (5-13), and (5-14) into Equation (5-11).

5.2 VOLUMETRIC LIQUID-SIDE MASS TRANSFER COEFFICIENT, k_La

The Transient Physical Gas Absorption technique [126, 127] was used to determine k_La. The decrease of the reactor pressure was recorded as a function of time during the transient absorption period, until equilibrium was reached. The calculation of the mass transfer coefficient of each component as a single-gas was performed from the decline of the total pressure of the gas as a function of time. For the gas mixture, the overall k_La of the mixture was first calculated for the decline of the total pressure as a function of time. Then, k_La for each component in the mixture was calculated from its corresponding partial pressure and diffusivity. The calculation details are given in the following.

5.2.1 Single-Gas Mass Transfer Coefficient

The two-film model was used to determine the rate of mass transfer of the gas into the liquid:

$$\frac{dn_L}{dt} = k_L a(C^* - C_L)V_L \quad (5\text{-}15)$$

A differential form of the general gas law, as shown in equation (5-16), can be used to determine the rate of solute gas uptake by monitoring the decline in pressure over time.

$$\frac{dn_L}{dt} = -\left(\frac{V_G}{ZRT}\right)\left(\frac{dP_{i,t}}{dt}\right) \tag{5-16}$$

C_L, the bulk concentration of the solute gas in the liquid-phase, can be expressed as follows:

$$C_L = \frac{V_G}{ZV_L RT}(P_{i,I} - P_{i,t}) \tag{5-17}$$

If the gas solubility at constant temperature is linear function of pressure, Henry's law can be written as:

$$He = \frac{P_{i,t}}{C^*} \tag{5-18}$$

Substituting Equations (5-16), (5-17), and (5-18) into Equation (5-15) yields the following equation:

$$-\frac{V_G}{ZRT}\frac{dP_{i,t}}{P_{i,t}\left(\frac{V_L}{He}+\frac{V_G}{ZRT}\right)-\frac{V_G P_{i,I}}{ZRT}} = k_L a dt \tag{5-19}$$

Let $Y = P_{i,t}\left(\frac{V_L}{He}+\frac{V_G}{ZRT}\right)-\frac{V_G P_{i,I}}{ZRT}$; This gives $dY = dP_{i,t}\left(\frac{V_L}{He}+\frac{V_G}{ZRT}\right)$

Equation (5-20) can be obtained by integrating between the limits of P_I at t = 0 and $P_{i,t}$ at any time (t):

$$\ln\left[\frac{P_{i,t}\left(\frac{V_L}{He}+\frac{V_G}{ZRT}\right)-\frac{V_G P_{i,I}}{ZRT}}{\frac{P_{i,I}V_L}{He}}\right] = -\left[\frac{V_L ZRT}{V_G He}+1\right]k_L a.t \tag{5-20}$$

By multiplying the numerator and denominator of the left-hand-side of Equation (5-20) by (ZRT/V_G) and rearranging, the following relationship can be obtained:

$$\ln\left[\frac{P_{i,t}(\psi+1)-P_{i,I}}{\psi P_I}\right]=-[\psi+1]k_L a.t \tag{5-21}$$

The function ψ is defined as $\psi = (V_L\ ZRT/V_G\ He)$.

At equilibrium where the pressure is ($P_{i,F}$), the final equilibrium concentration (C^*_{eq}) is defined as follows:

$$C^*_{eq}=\frac{V_G}{V_L ZRT}(P_{i,I}-P_{i,F}) \tag{5-22}$$

Also, C^*_{eq} can be expressed as:

$$C^*_{eq}=\frac{P_{i,F}}{He} \tag{5-23}$$

By equating equations (5-22) and (5-23), one can obtain:

$$\frac{P_{i,I}-P_{i,F}}{P_{i,F}}=\frac{V_L ZRT}{HeV_G}=\psi \tag{5-24}$$

By substituting Equation (5-24) into (5-21) and multiplying the left-hand-side of Equation (5-21) by $(P_{i,F}/P_{i,I})$, the following working equation can be obtained:

$$\frac{P_{i,F}}{P_{i,I}}ln\left[\frac{P_{i,I}-P_{i,F}}{P_{i,t}-P_{i,F}}\right]=k_L a\ t \tag{5-25}$$

If k_La is a constant, Equation (5-25) becomes a linear function of time and can be written as:

$$F(t)=k_L a\ t \tag{5-26}$$

If the left side of Equation (5-26) is plotted versus time and a linear relationship is obtained, the slope of the line will be k_La.

5.2.2 Gas Mixture Mass Transfer Coefficients

For a gas mixture, a different approach was used since the value of $P_{i,t}$ is unknown. Therefore, the mass transfer rate of each gas into the liquid is written as:

$$\frac{dn_{i,L}}{dt} = k_L a_i (C_i * - C_{i,L}) V_L \tag{5-27}$$

The total mass transfer rate for all components can be expressed as:

$$\frac{dn_L}{dt} = \sum_i \frac{dn_{i,L}}{dt} = \sum_i k_L a_i \ (C_i * - C_{i,L}) V_L \tag{5-28}$$

A differential form of the general gas law, is used to represent the rate of solute gas uptake by the liquid, by monitoring the decline of pressure as a function of time:

$$\frac{dn_L}{dt} = -\frac{dn_G}{dt} = -\frac{d}{dt}\left(\frac{P_G V_G}{ZRT}\right) \tag{5-29}$$

This leads to the following equation:

$$-\frac{d}{dt}\left(\frac{P_G V_G}{ZRT}\right) = \sum_i k_L a_i \ (C_i^* - C_{i,L}) V_L \tag{5-30}$$

At every pressure, C_i* can be estimated from the experimental C* values of N_2 and He obtained in the Silicone oil and SpectraSyn Polyalphaolefin. The $k_L a$ of He and N_2 can be estimated by solving numerically Equation (5-30).

Also, if the overall $k_L a$ for the binary gaseous mixture is obtained in a given liquid using Equation (5-25), the $k_L a$ for He and N_2 in the mixture can be calculated from the following two equations [128]:

$$\frac{(k_L a)_{He}}{(k_L a)_{overall}} = \frac{C_{He}^* \sqrt{D_{He}}}{C_{He}^* \sqrt{D_{He}} + C_{N_2}^* \sqrt{D_{N_2}}} \tag{5-31}$$

Where D_{He} and D_{N2} are the diffusivities of He and N_2 in the liquid, respectively.

6.0 RESULTS AND DISCUSSION

In the following section, experimental results for the gas solubility (C*) and volumetric mass transfer coefficient (k_La) for N_2, He and their mixtures, in the two liquids Silicone Oil and SpectraSyn Polyalphaolefin are presented. The data were obtained in a one-gallon Autoclave reactor operated in the GIR mode over the range of operating conditions listed in Table 4-1.

6.1 C* IN SILICONE OIL AND SPECTRASYN POLYALPHAOLEFIN

6.1.1 Reproducibility of C*

Figures 6-1 and 6-2 show the reproducibility of the solubilities of N_2 in Silicone Oil and SpectraSyn Polyalphaolefin, and as can be seen the data can be correlated with an R^2 value of 0.987 and 0.992, respectively. Equation (6-1) was used to calculate R^2, which is the coefficient of determination.

$$R^2 = 1 - \frac{\sum_i^k (C^*_{exp,i} - C^*_{predicted,i})^2}{\sum_i^k (C^*_{exp,i} - C^*_{Average})^2} \qquad (6\text{-}1)$$

The calculated Average Absolute Relative Error (AARE), define by Equation (6-2), for *C** of N_2 in the Silicone oil and SpectraSyn polyalphaolefin was 4.50% and 4.29%, respectively.

$$AARE = \frac{\sum_i^k \left| \frac{(C^*_{predicted,i} - C^*_{exp,i})}{C^*_{exp,i}} \right|}{\sum_i^k n_i} \quad (6\text{-}2)$$

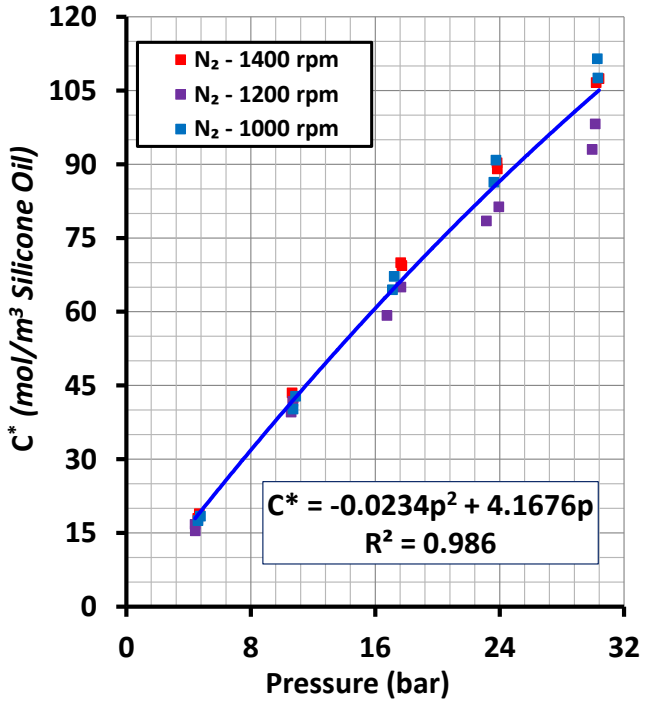

Figure 6-1: Reproducibility of N_2 Solubility in Silicone Oil at 348 K

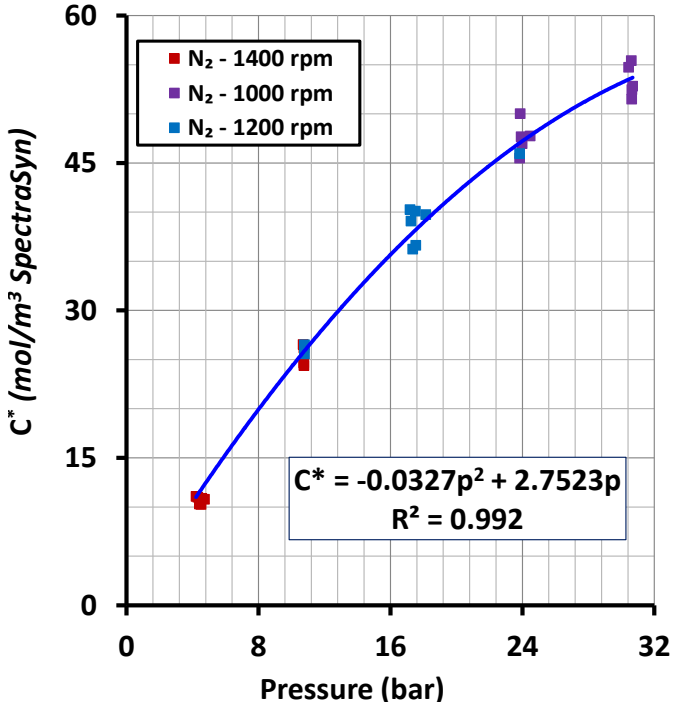

Figure 6-2: Reproducibility of N_2 Solubility in SpectraSyn Polyalphaolefin At 348 K

6.1.2 Effect of Pressure and Temperature on C*

The effect of the gas partial pressure of He and N_2 on their C* values in the Silicone Oil and SpectraSyn Polyalphaolefin is shown in Figures 6-3 and 6-4 and as can be observed C* values increase with the gas partial pressure. Also, the effect of temperature on the solubilities of He and N_2 in the two liquid can be pointed out by comparing Figures 6-3 and 6-4 and as can be seen, C* values for both gases increase with increasing temperature.

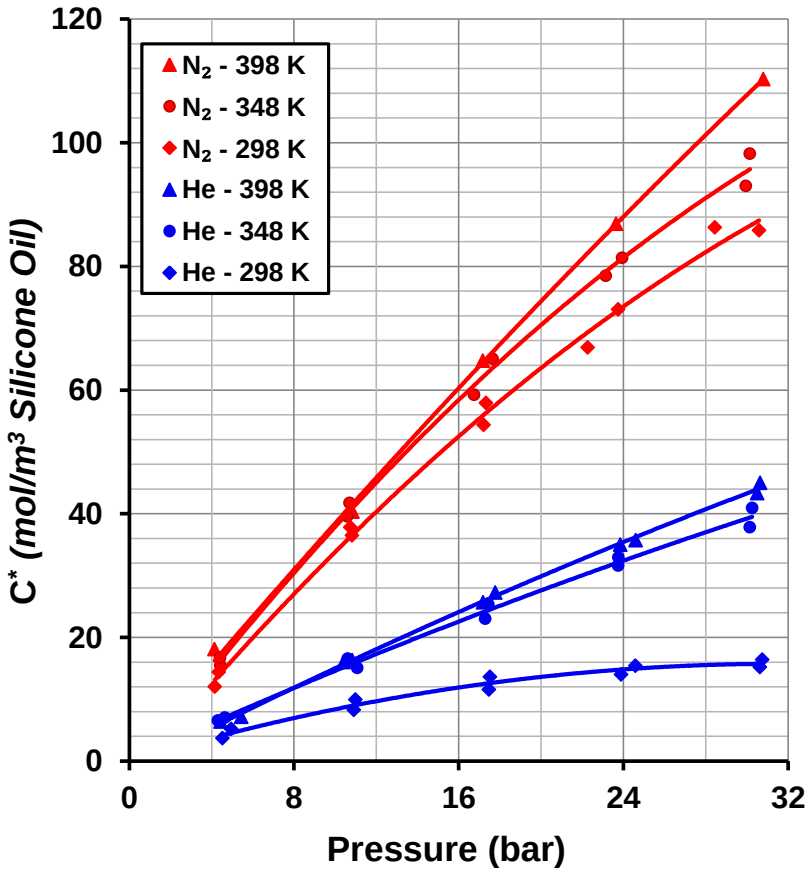

Figure 6-3: Effect of Pressure and Temperature on C* of He and N_2 in Silicone Oil at 1200 rpm

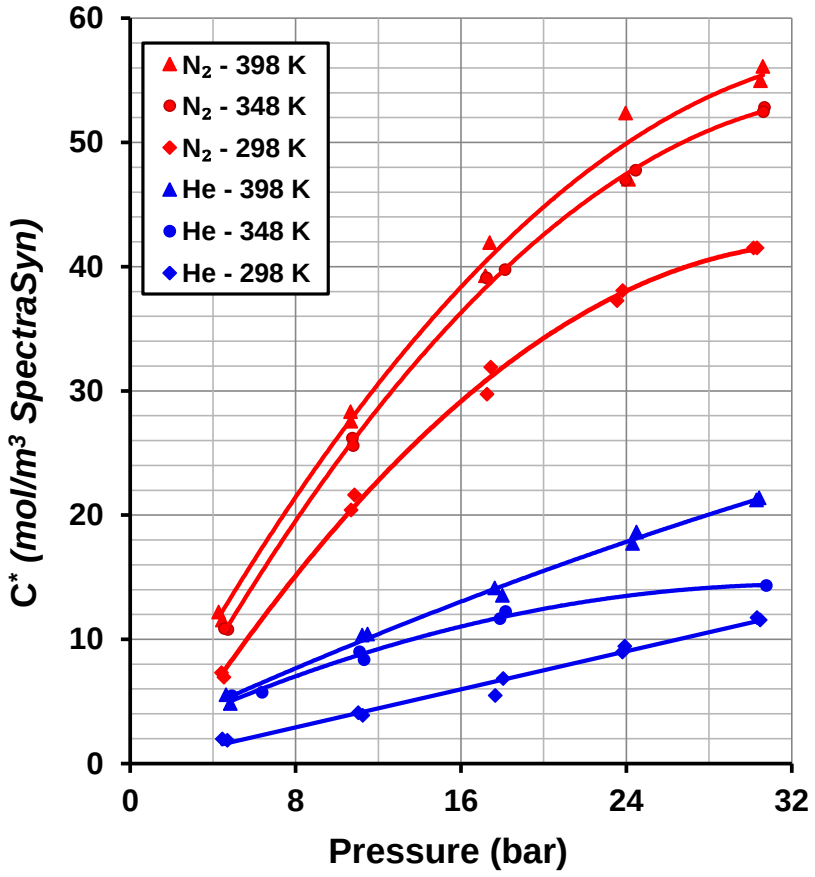

Figure 6-4: Effect of Pressure and Temperature on C* of He and N_2 in SpectraSyn Polyalphaolefin at 1200 rpm

6.1.3 Correlations of C* Values

Due to the non-linear behavior of C* values with pressure, Henry's Law was not applicable. Instead, Equation (6-3) was used to represent the dependency of C* on the equilibrium final gas partial pressure.

$$C^* = E_0 P_{i,F} + E_1 P_{i,F}^2 \qquad (6\text{-}3)$$

The values of the coefficients in Equation (6-3) are calculated at different temperatures and listed in Table 6-1 for He and N_2 in the Silicone Oil and the SpectraSyn Polyalphaolefin.

Table 6-1: Coefficients in Equation (6-3)

Gas	Temperature (K)	Silicone Oil		SpectraSyn	
		$E_0\ \left(\frac{mol}{m^3 \cdot bar^2}\right)$	$E_1\ \left(\frac{mol}{m^3 \cdot bar}\right)$	$E_o\ \left(\frac{mol}{m^3 \cdot bar^2}\right)$	$E_1\ \left(\frac{mol}{m^3 \cdot bar}\right)$
He	298	0.996	-0.0158	0.337	-0.0016
	348	1.534	-0.0076	0.974	-0.0167
	398	1.545	-0.0032	0.987	-0.0097
N_2	298	3.662	-0.0256	0.2220	-0.0275
	348	4.168	-0.0234	0.2752	-0.0327
	398	3.973	-0.0127	0.3018	-0.0393

6.1.4 Effect of Gas and Liquid Natures on C*

Figures 6-3 and 6-4 show the effect of gas nature on the equilibrium solubilities of He and N_2 in Silicone Oil and SpectraSyn Polyalphaolefin. As can be seen in these figures, the solubilities of N_2 appear to be greater than those of He under similar operating conditions. Also, the effect of liquid nature on *C** can also obtained by comparing Figure 6-1 with Figure 6-2 for Silicone Oil and SpectraSyn Polyalphaolefin, respectively. As can be observed under similar conditions, the solubilities of the two gases are greater in Silicone Oil than in SpectraSyn Polyalphaolefin.

This behavior can be explained using the Hildebrand solubility parameter (δ), which is determined from the molar heat of vaporization (H_v) and the molar volume (v) using Equation (6-4):

$$\delta = \sqrt{\frac{H_v - RT}{v}} \qquad (6\text{-}4)$$

The solubility of component 1 in a binary mixture, expressed as a mole fraction (x_1), can be related to the solubility parameters of the two components at a given temperature (T) by the following equation:

$$x_1 \propto \exp\left(-\frac{v_1 * (\delta_1 - \delta_2)^2}{RT}\right) \quad (6\text{-}5)$$

Where $v_1\ is$ the molar volume of component 1; and δ_1 and δ_2 are the solubility parameters of components 1 and 2, respectively.

Table 6-2 shows the calculated solubility parameters for the two gases and two liquids used at different temperatures. It should be mentioned that corresponding H_v and v values for the two liquids were estimated using the asymptotic behavior correlations by Marano et al. [123].

Table 6-2: Hildebrand Solubility Parameters for the Two Liquids

Species	Solubility Parameter $(MPa)^{0.5}$				
	298 K	**323 K**	**348 K**	**373 K**	**398 K**
He	0.0117	0.0117	0.0117	0.0117	0.0117
N_2	0.354	0.331	0.309	0.285	0.262
Silicone Oil	11.944	11.811	11.677	11.542	11.460
SpectraSyn Polyalphaolefin	21.239	21.022	20.804	20.583	20.361

According to Equation (6-5), x_1 is inversely proportional to the difference between δ_1 and δ_2 provided that v_1 and T are the same, which means that a smaller difference between δ_1 and δ_2 should result in a higher value x_1. Thus, the values of the solubility parameters listed in Table 6-2 can be used to explain the observed behavior of the solubility of the He and N_2 in the Silicone Oil and SpectraSyn Polyalphaolefin. For instance, N_2 has systematically greater solubility values than He in the two liquids. Also, the solubilities of He and N_2 are greater in the Silicone Oil than in the SpectraSyn Polyalphaolefin.

6.2 k_La IN SILICONE OIL AND SPECTRASYN POLYALPHAOLEFIN

The volumetric liquid-side mass transfer coefficients of He, N_2 and their mixtures were measured in Silicone Oil and SpectraSyn Polyalphaolefin over the range of operating conditions listed in Table 4-1. The results are discussed in the following.

6.2.1 Effect of Pressure and Mixing Speed on k_la

Figures 6-5 and 6-6 show the effect of pressure on k_La at 348 K in both Silicone Oil and SpectraSyn Polyalphaolefin, and as can be seen k_La values appear to increase with increasing pressure. These data are in agreement with numerous findings reported by several investigators [56-63] as listed in Table 2-2. They also related this increase of k_La to the decrease of the liquid-phase surface tension and viscosity with increasing the amount of dissolved gas (i.e., the gas solubility) with increasing pressure. The decrease of the liquid viscosity and surface tension result in small gas bubbles with large gas-liquid interfacial area (a), and subsequently k_La.

Figures 6-5 and 6-6 also show the effect of mixing speed on k_La at 348 K in both Silicone Oil and SpectraSyn Polyalphaolefin; and as can be observed k_La values increase with the mixing speed. These data are in accord with many literature findings [56-65, 67, 69, 71-75] as given in Table 2-4. This behavior was attributed to the increased amount of induced gas into the liquid with increasing mixing speeds, which resulted in increasing the gas holdup and hence the gas-liquid interfacial area (a). Moreover, increasing mixing speed increased the turbulence and shear rate which, according the two film theory, decrease the liquid film thickness and increase k_L. Thus, increasing k_L and a led to the increase of k_La with mixing speed.

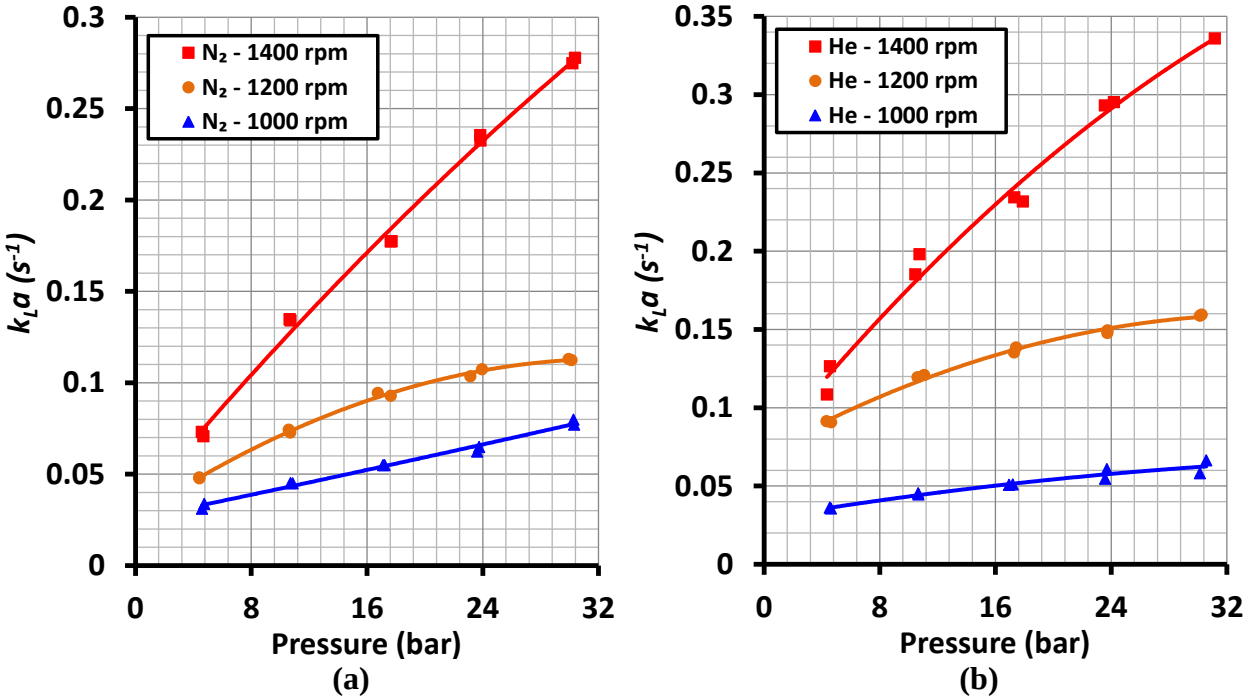

Figure 6-5: Effect of Pressure and Mixing Speed on k_La of N_2 (a) and He (b) in Silicone Oil at 348 K

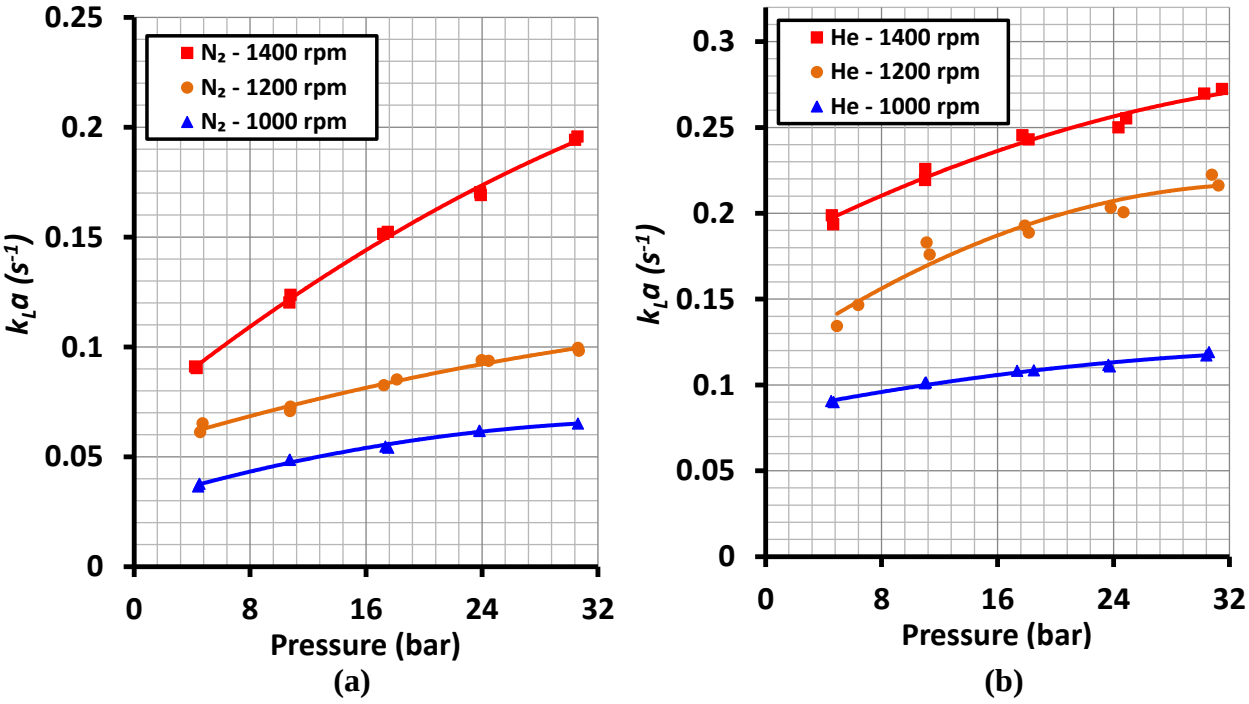

Figure 6-6: Effect of Pressure and Mixing Speed on k_La of N_2 (a) and He (b) in SpectraSyn Polyalphaolefin at 348 K

6.2.2 Effect of Temperature on k_La

Figures 6-7 and 6-8 show the effect of temperature on k_La values at 1200 rpm for N_2 and He in the Silicone Oil and SpectraSyn Polyalphaolefin, respectively. As can be seen in these figures, k_La values for both gases in the two liquids increase with temperature. Also, in the Silicone Oil, the increase of k_La values from 298 to 348 K was smaller when compared with that from 298 to 348 K. This k_La behavior is in agreement with that reported in the literature by numerous investigators [56, 58, 61, 63, 64, 66, 67, 69] as given in Table 2-3. The increase of k_La values with temperature was attributed to the decrease of the liquid viscosity and surface tension, resulting in a decrease of the average bubble size and accordingly an increase of the interfacial area, a. In addition, increasing temperature increases the gas diffusivity into the liquid and hence k_L. This is because k_L is proportional to the diffusivity to the power 0.5 (penetration theory) to 1.0 (two-film theory). Thus, the increase of a and k_L led to the increase of k_La.

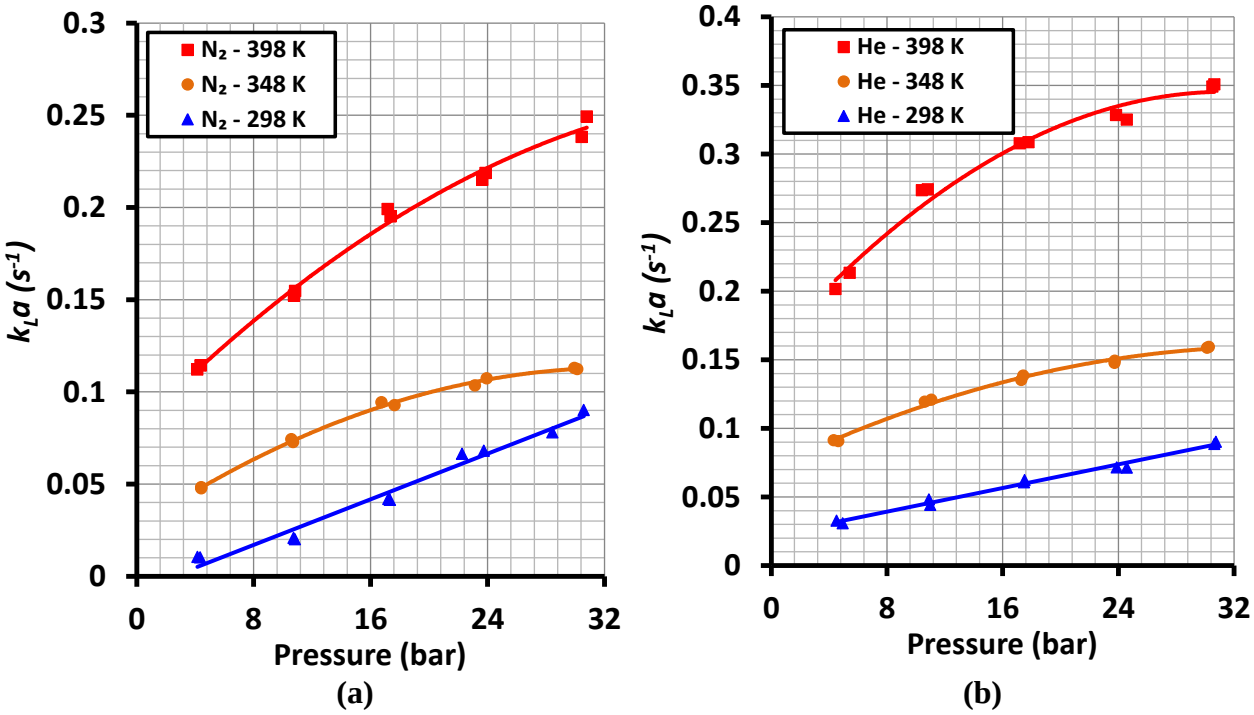

Figure 6-7: Effect of Temperature on k_La of N_2 (a) and He (b) in Silicone Oil at 1200 rpm

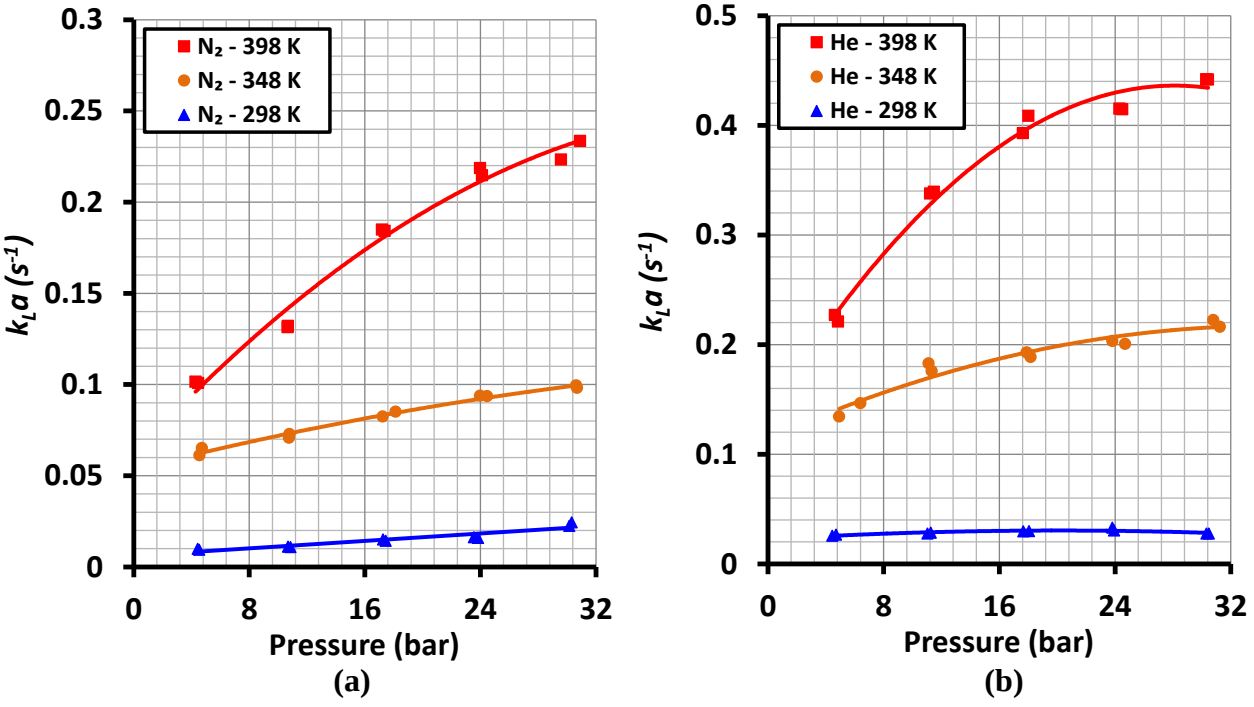

Figure 6-8: Effect of Temperature on k_La of N_2 (a) and He (b) in SpectraSyn Polyalphaolefin at 1200 rpm

6.2.3 Effect of Gas Nature on k_La

Figures 6-9 to 6-11 show the effect of gas nature on k_La values of He, N_2 and their mixtures in Silicone Oil and SpectraSyn Polyalphaolefin; and as can be observed k_La values for He as a single-gas are much greater than those for N_2 as single-gas. Also, k_La values for the 50/50 and 75/25 gaseous mixtures lie between those for N_2 and He as single gases. This behavior can be attributed to the fact that at the same temperature, the diffusivity values of He are consistently greater than those of N_2 in the Silicone Oil and SpectraSyn Polyalphaolefin as shown in Figures 4-11 and 4-12, respectively. Moreover, for the 50/50 by volume He and N_2 gaseous mixture, overall k_La for this pseudo-gas, with an apparent molecular weight of about 16 kg/kmol, lies between those of He and N_2.

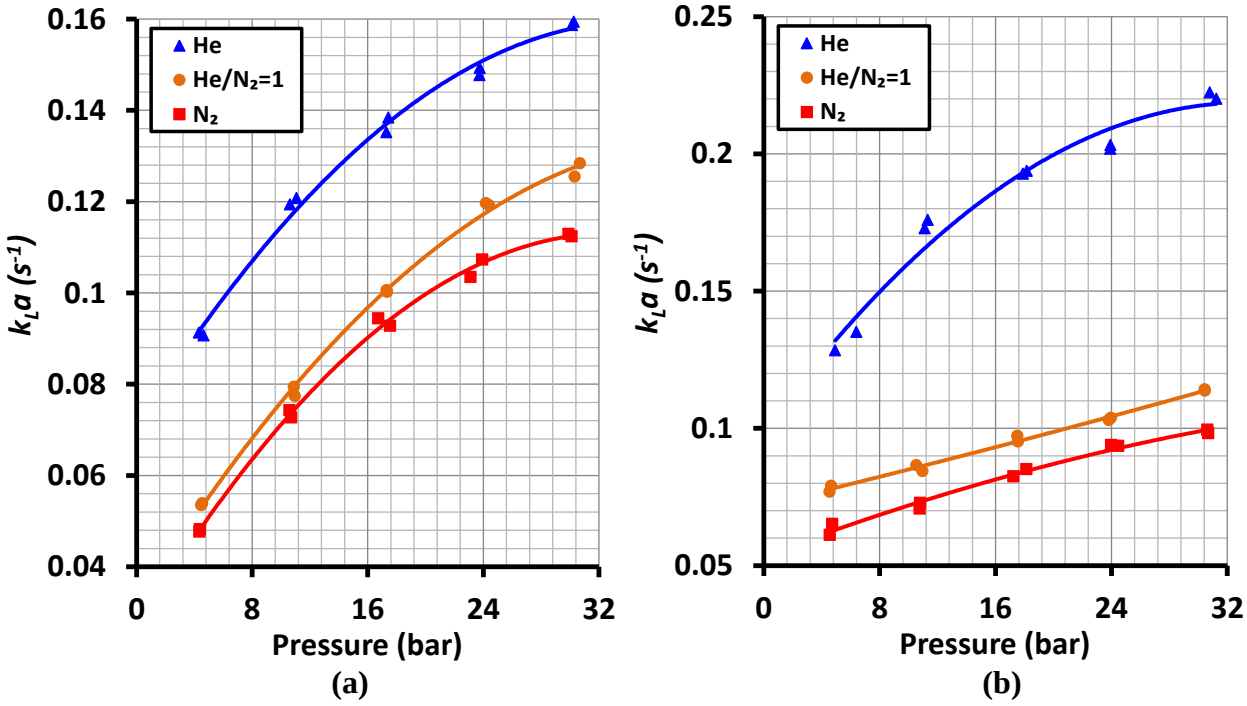

Figure 6-9: Effect Gas Nature on k_La of N_2 and He in Silicone Oil (a) and SpectraSyn Polyalphaolefin (b) at 348 K and 1200 rpm

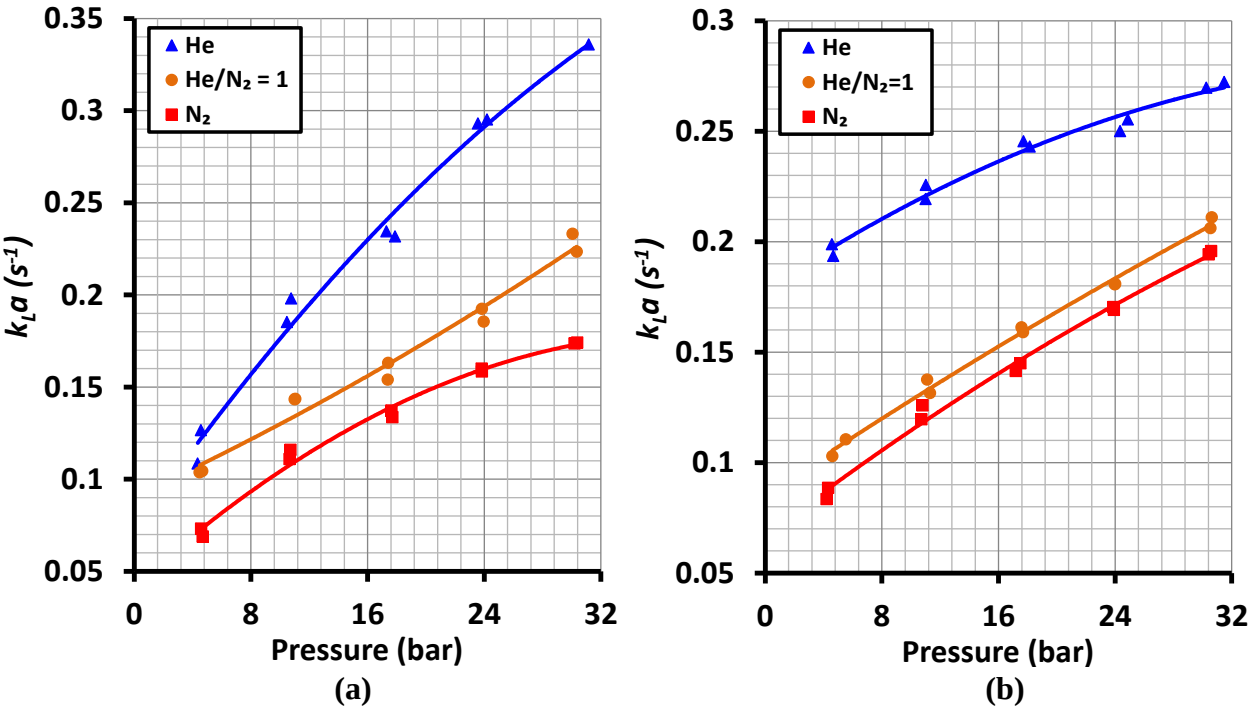

Figure 6-10: Effect Gas Nature on k_La of N_2 and He in Silicone Oil (a) and SpectraSyn Polyalphaolefin (b) at 348 K and 1400 rpm

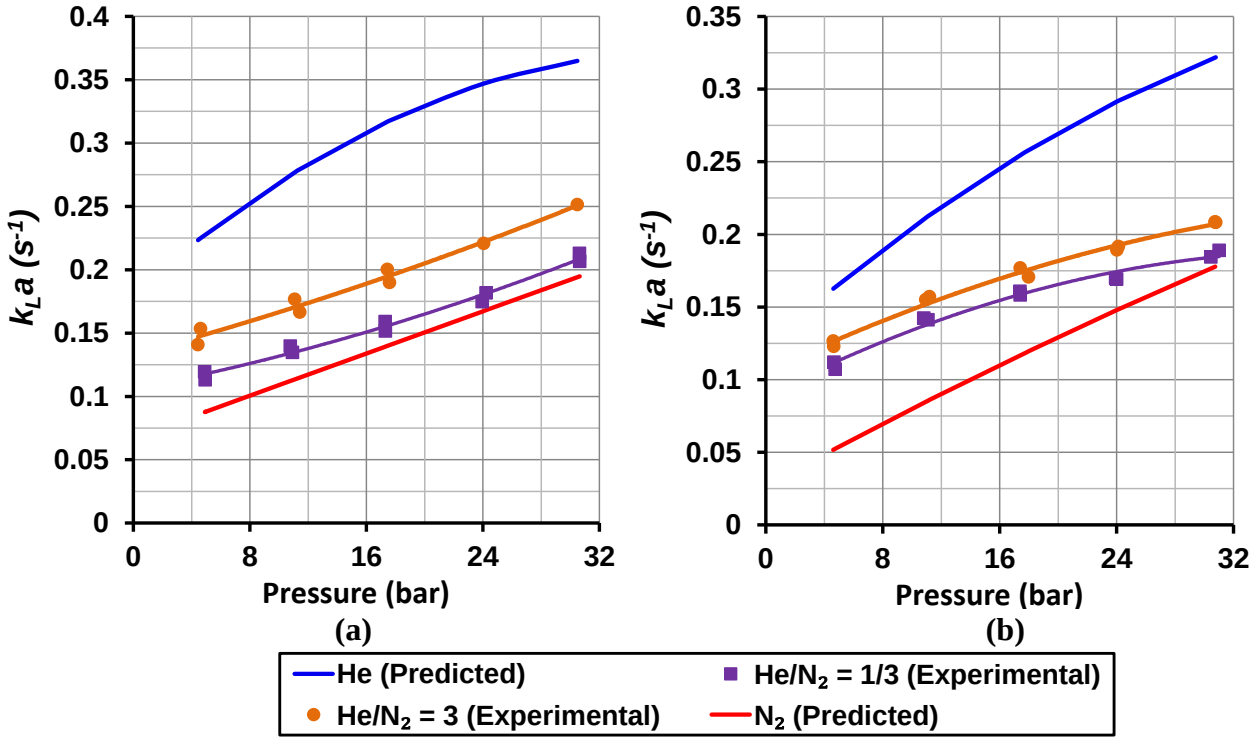

Figure 6-11: Effect Gas Nature on k_La of N_2 and He in Silicone Oil (a) and SpectraSyn Polyalphaolefin (b) at 373 K and 1300 rpm

6.2.4 Effect of Liquid Nature on k_La

Figures 6-12 and present the effects of liquid nature on k_La values of N_2 and He at 398 K and 1200 rpm. In order to explain the effect of liquid nature on k_La, one should recall Figures 4-5, 4-6, 4-11, 4-12, 6-3 and 6-4. Figures 4-5 and 4-6 show the viscosity values of Silicone Oil are greater than those of SpectraSyn Polyalphaolefin; Figures 4-11 and 4-12 show the diffusivity values of N_2 and H_2 in Silicone Oil are lower than those in SpectraSyn Polyalphaolefin; and Figures 6-3 and 6-4 show the C* values of N_2 and He in Silicone Oil are greater than those in SpectraSyn Polyalphaolefin. The lower N_2 and He diffusivities in Silicone Oil than those in SpectraSyn Polyalphaolefin suggest that their corresponding liquid-side mass transfer coefficients (k_L) are lower in Silicone Oil than those in SpectraSyn Polyalphaolefin. Also, the higher viscosities of Silicone Oil than those of SpectraSyn Polyalphaolefin hinder the flow of the induced gas bubbles, forcing them to coalesce into large bubbles with small gas-liquid interfacial area (a). This means that k_La values in Silicone Oil are expected to be lower than those in SpectraSyn Polyalphaolefin, which is evident in Figures 6-12 and . However, the behavior of the induced gas bubbles appears to strongly dependent on their mass, as heavier bubbles, such as N_2 bubbles when compared with those of He, are easily broken by the impeller and dispersed throughout the reactor, increasing their gas-liquid interfacial area (a). It seems that the increase of the gas-liquid interfacial area in the case of N_2 overcame the decrease of k_L, leading to greater N_2 k_La values in Silicone Oil than those in the SpectraSyn Polyalphaolefin as shown in Figures 6-12 and .

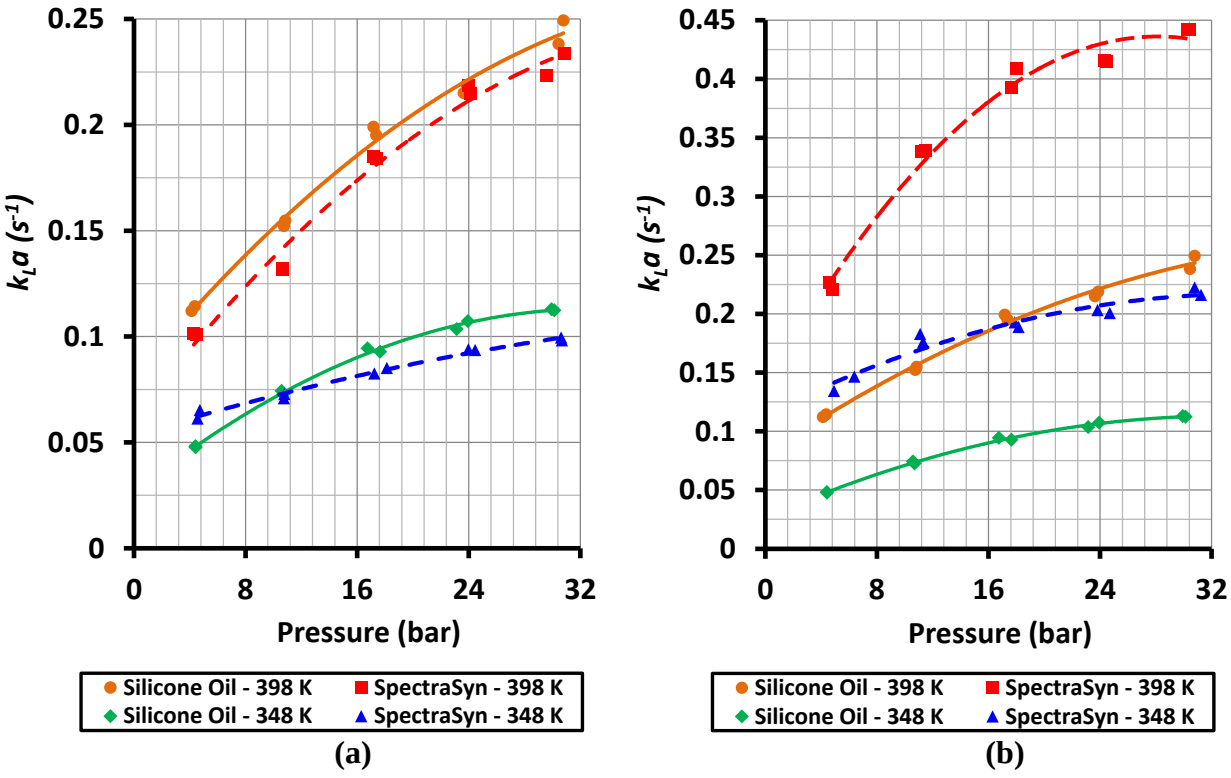

Figure 6-12: Effect of Liquid Nature at Different Temperatures on k_La of N_2 (a) and He (b) at 1200 rpm

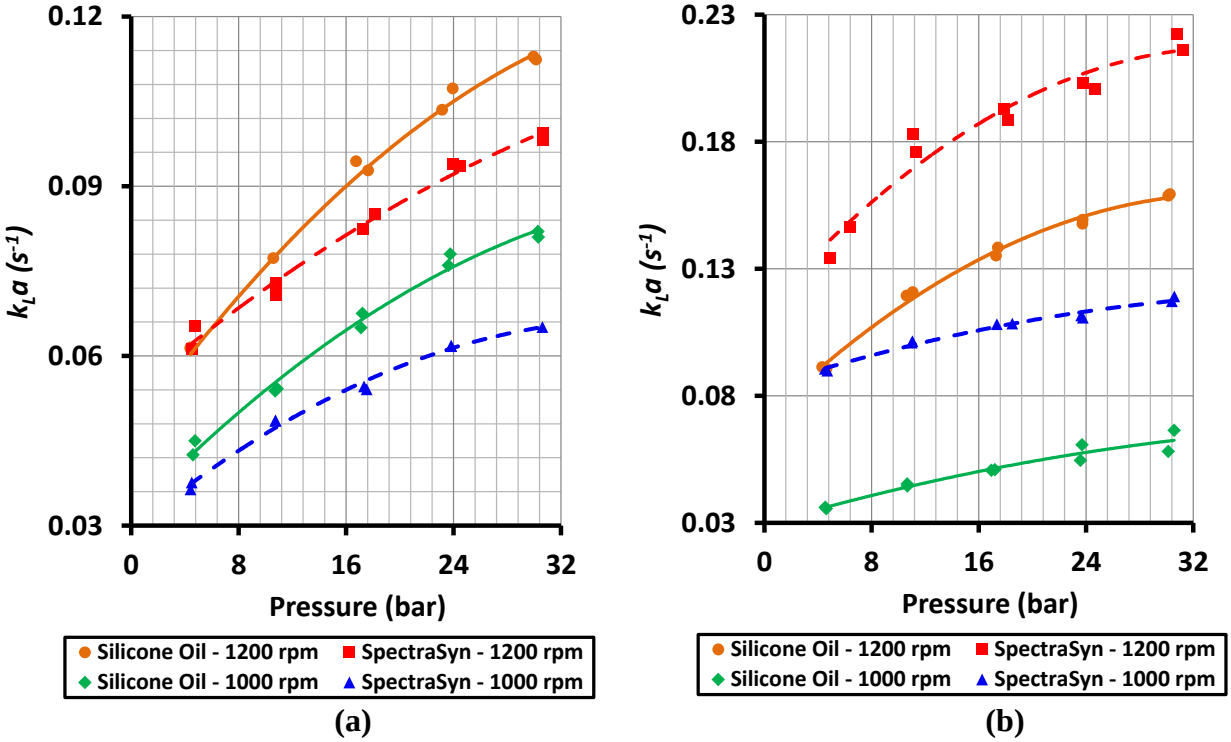

Figure 6-13: Effect of Liquid Nature at Different Mixing Speeds on k_La of N_2 (a) and He (b) at 348 K

6.3 STATISTICAL CORRELATIONS OF k_La

The experimental k_La obtained for N_2 and He in both Silicone Oil and SpectraSyn Polyalphaolefin were statistically correlated and Equation (6-6) was developed to fit the data shown in Figures 6-12 and and the coefficients in this equation are listed in Table 6-3. Equation (6-6) appears to fit the experimental data with high accuracy as shown in Figure 6-14. The Standard deviation (σ) calculated using (6-7) is 1.14%.

$$k_La = \alpha_1 - \alpha_2 N - \alpha_3 P - \alpha_4 T + \alpha_5 N^2 - \alpha_6 P^2 + \alpha_7 T^2 + \alpha_8 (N \cdot P) + \alpha_9 (P \cdot T) \quad (6\text{-}6)$$

$$\sigma = \sqrt{\frac{1}{K}\sum_{i=1}^{K}(x_i - \bar{x})^2} \quad (6\text{-}7)$$

Table 6-3: Coefficients in in Equation (6-6)

Coefficient ($\times 10^{-3}$)	**SpectraSyn Polyalphaolefin**		**Silicone Oil**	
	He	**N_2**	**He**	**N_2**
$\boldsymbol{\alpha_1}$	-1204	1261	2358772	2000
$\boldsymbol{\alpha_2}$	1.328	-1.013	-878	-1.709
$\boldsymbol{\alpha_3}$	-25.03	-30.21	-24583	-19.81
$\boldsymbol{\alpha_4}$	0.1	-4.44	-12630	-6.75
$\boldsymbol{\alpha_5}$	0.000448	0.000465	0.43	0.00073
$\boldsymbol{\alpha_6}$	-0.1349	0.0162	-86.5	-0.0331
$\boldsymbol{\alpha_7}$	0.00272	0.00714	20.74	0.01124
$\boldsymbol{\alpha_8}$	0.00445	0.00751	17.36	0.01537
$\boldsymbol{\alpha_9}$	0.07879	0.06776	30.17	0.01878

It should be mentioned that in Equation (6-6) is limited to the experimental data and operating conditions used in this study.

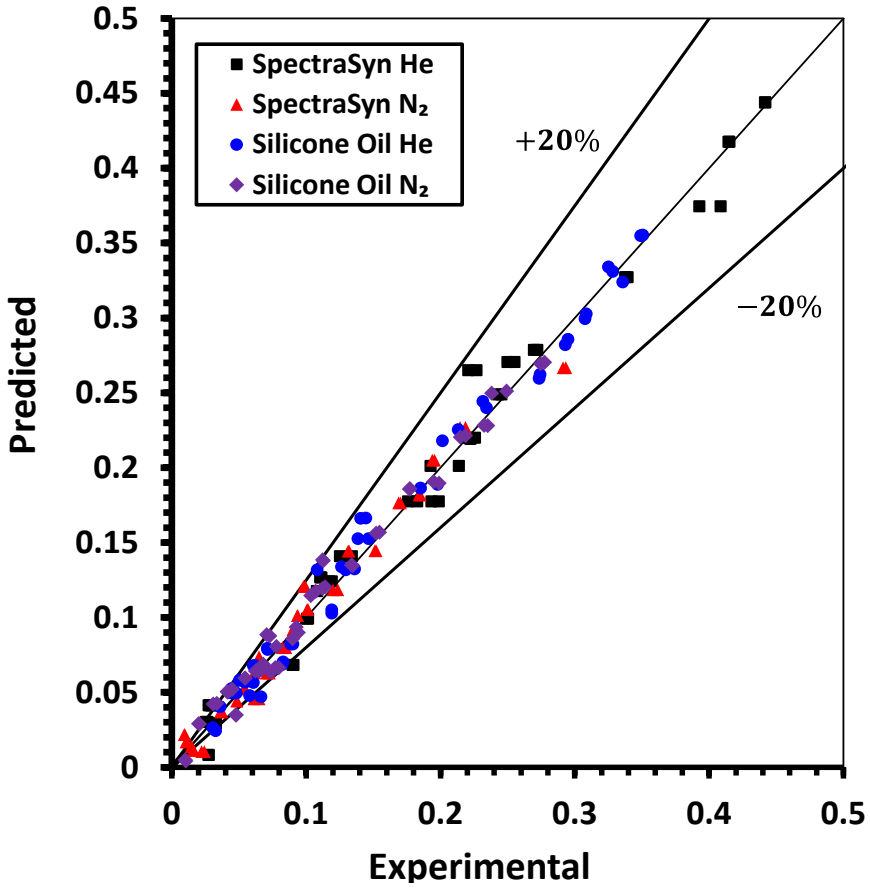

Figure 6-14: Comparison between Experimental and Predicted $k_L a$ Values Using Equation (6-6)

6.4 FEASIBILITY OF USING DIFFERENT STARTUP LIQUIDS IN F-T SBCRs

To further investigate the feasibility of using Silicone Oil and SpectraSyn as startup liquids in F-T SBCRs, an unsteady state vapor liquid equilibrium (VLE) model was developed. The model is based on the previous works of Raje and Davis [130] and Caldwell and Van Vuuren [131]. The model is based on the following assumptions:

(1) The ASF distribution, described by a single α value, is valid and accordingly the mole fraction of an individual component (*i*) can be expressed by Equation (6-8):

$$z_i = (1-\alpha)\alpha^{i-1} \tag{6-8}$$

(2) The hydrocarbon products consist exclusively of paraffins, between C_1-C_{45}.

(3) The entire system is at VLE

(4) The vapor-phase follows the ideal gas law and the liquid-phase behaves ideally, i.e., Raoult's law is applicable:

$$y_i P = x_i P^v \tag{6-9}$$

Where y_i and x_i are the mole fractions of component *i* in the vapor- and liquid-phase; and *P* and P^v are the total pressure and vapor pressure, respectively.

(5) The liquid product stream is continuously withdrawn in order to continuously maintain a constant amount of liquid inside the reactor.

(6) The mass of the liquid inside the reactor remains constant. Ideally, a constant volume has to be considered, however, this assumption is planned as a future improvement.

The vapor pressure of each hydrocarbon component can be calculated using the correlation by Caldwell and Van Vuuren [131] which is valid up to C_{50} [34, 130]. This correlation is shown in Equations (6-10) through (6-13).

$$P^{v} = P_o \beta^{i-1} \tag{6-10}$$

$$P_o = 1.78382\text{x}10^{4} \quad kPa \tag{6-11}$$

$$\beta = \exp\left(-427.218\left(\frac{1}{T} - 1.029807\text{x}10^{-3}\right)\right) \tag{6-12}$$

The rate of CO conversion to n-alkanes is given by:

$$r = F(y_{CO})X_{HC} = \frac{F(X_{CO+H_2})}{(4-\alpha)} \tag{6-13}$$

Where F is the molar feed rate into the reactor, y_{CO} is the mol fraction of CO in the feed; and X_{HC} and X_{CO+H_2} are the CO conversion and overall syngas conversions, respectively.

Therefore, the overall unsteady state hydrocarbon mole balance is:

$$\frac{d(Q)}{dt} = F(1 - 2y_{CO}X_{HC}) - V + L \tag{6-14}$$

Where Q is the number of moles of the liquid inside the reactor; and V and L are the molar flow rates of vapor and liquid leaving the reactor, respectively.

Consequently, the unsteady state mole balance for a hydrocarbon component i is:

$$\frac{d(Qx_i)}{dt} = r(1-\alpha)z_i - Vy_i + Lx_i \tag{6-15}$$

The above equations were integrated numerically with the assumption that at the initial condition, the reactor contained only the Startup liquid, and the expected changes in liquid composition are not expected to affect the conversion or selectivity. In addition, to close the solution, the following constraint was held:

$$Q\sum Mw_i x_i = Q_o Mw_{startup\ liquid} \tag{6-16}$$

Where Q_o stands for the initial number of moles of the liquid inside the reactor.

In this analysis, 5 liquids, namely Silicone oil, SpectraSyn polyalphaolefin, reactor wax, n-tetradecane and paraffins mixture, were used. Some properties of these liquids are given in Table 6-4. The calculations were conducted at 410 K and 15 bars, and the equations were discretized in time with a time step of 0.01, for a startup period of 200 h. The results of the calculations are shown in Figures 6-15 and 6-16 for α values of 0.92 and 0.85, respectively. As can be seen in these figures, SpectraSyn polyalphaolefins remains in the reactor for the longest time (> 200 hr) when used as a startup liquid, whereas the Paraffins mixture remains for the shortest times during startup (~100 hr). This behavior can be related to the highest moleacular weight of the SpectraSyn polyalphaolefins as given in Table 6-4. It seems that the molecular weight is the main factors controlling the residence time of the startup liquid in the SBCRs.

Table 6-4: Properties of the Liquids used in this Analysis

	MW (kg/kmol)	ρ (kg/m^3) at 410 K	P^v (bar) at 410 K
Paraffins Mixture	176.36	602.99	1.0782
n-Tetradecane	198.64	578.0	0.5223
Silicone Oil	236.53	804.05	0.1673
Reactor Wax	408.08	682.56	0.01055
SpectraSyn Polyalphaolefin	606.14	675.88	0.00716

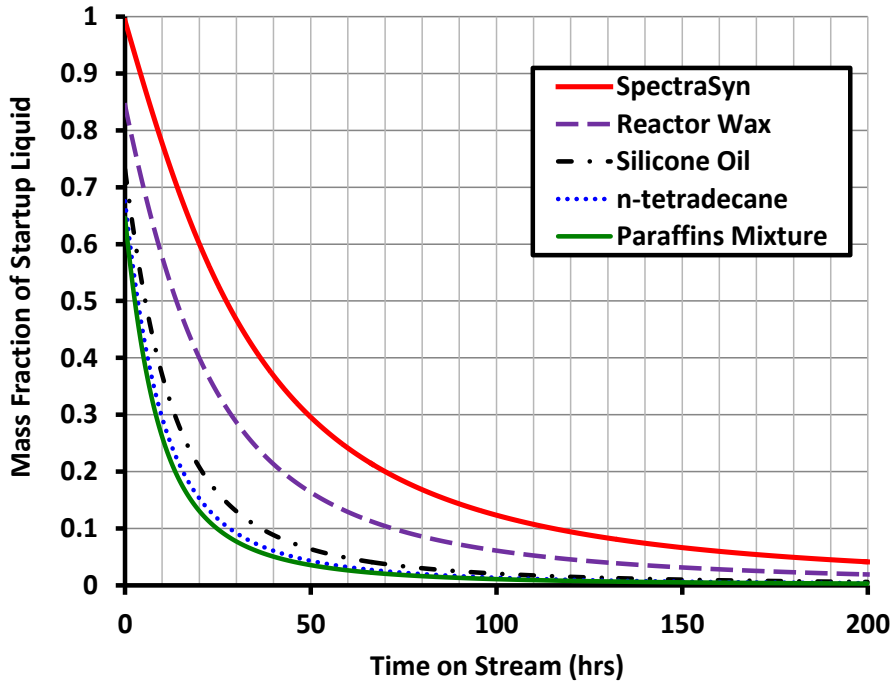

Figure 6-15: Change in Startup Liquid Mass Fraction with Time for $\alpha = 0.92$ at T=410 K

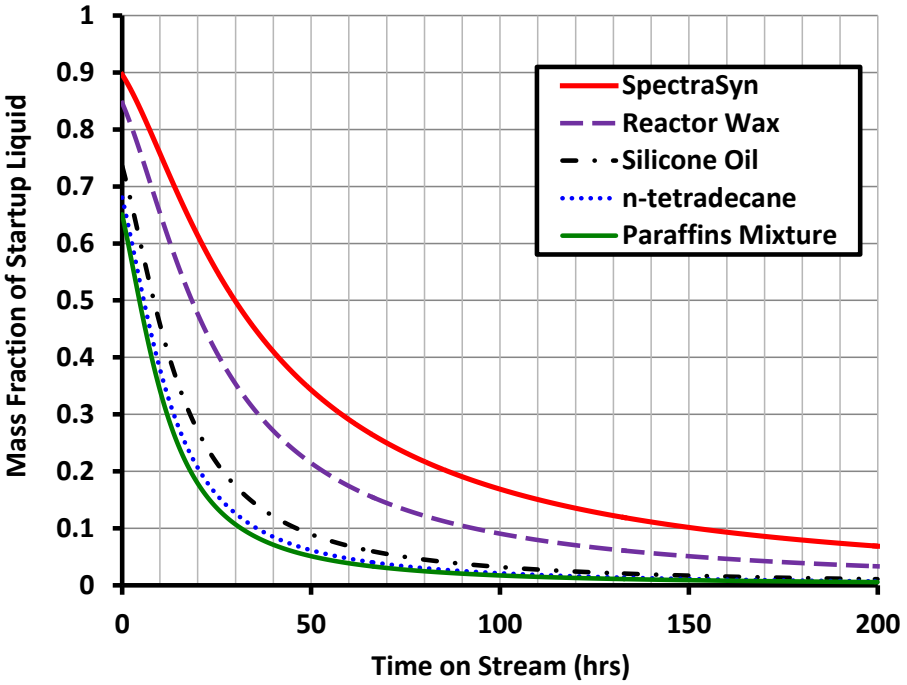

Figure 6-16: Change in Startup Liquid Mass Fraction with Time for $\alpha = 0.85$ at T=410 K

7.0 CONCLUSIONS

The equilibrium solubilities (C*) and volumetric liquid-side mass transfer coefficients (kLa) for He and N_2, as surrogates to H_2 and CO, and their mixtures (25% He/75% N_2, 50% He/50% N_2, 75% He/25% N_2) were measured in two different liquids (Silicone Oil and SpectraSyn polyalphaolefin) as startup liquids in Fischer-Tropsch Slurry Bubble Column Reactors (SBCRs). The data were obtained within wide ranges of pressures (4-30 bar), temperatures (298-398 K) and mixing speeds (1000-1400 rpm) in an agitated ZipperClave reactor operating in a gas-inducing mode. The effects of different operating variables as well as gas and liquid nature on C* and k_La for He and N_2 in the two liquids were discussed. Also, the feasibility of using different liquids as startup liquids for F- synthesis in SBCRs were explored. The interpretation of the experimental results and the calculations led to the following conclusions:

1. At constant temperature, the C* values of He and N_2 in the Silicone Oil and SpectraSyn polyalphaolefins increased non-linearly with the gas partial pressure and hence Henry's Law was not applicable.
2. Under similar pressures and temperatures, the C* values of He and N_2 in the Silicone Oil were greater than those in the SpectraSyn polyalphaolefins; and C* values of N_2 were greater than those of He in both liquids. This behavior was attributed to the differences among the Hildebrand solubility parameters calculated for the gases and liquids used.

3. The k_La values of both He and N_2 in the two liquids increased with the mixing speed, gas partial pressure and system temperature which was related to the increase of both the gas-liquid interfacial area (a) and the liquid-side mass transfer coefficient (k_L). Increasing mixing speed, gas partial pressure and system temperature increased the gas holdup and decreased the liquid-phase viscosity and surface tension, leading to the formation of small gas bubbles and hence an increase of (a). Also, increasing mixing speed and system temperature increased the turbulence and the gas diffusivity in the liquid, resulting in an increase of (k_L).
4. Under similar pressure, temperature and mixing speed, the k_La values of He in the two liquids were greater than those of N_2. This behavior was because the diffusivities of He in both liquids were greater than those of N_2 at the same temperature and hence $(k_L)_{He}$ and consequently $(k_La)_{He}$ should be greater than those of N_2 in both liquids, knowing that $k_L \propto (D_{AB})^n$, where n = 1for the two-film theory, and 0.5 for the penetration theory.
5. Unlike gas solubilities, k_La values of He were lower in Silicone Oil than those in the SpectraSyn Polyalphaolefin, whereas the opposite was true in the case of N_2. This behavior was attributed to the lower He and N_2 diffusivities in Silicone Oil than in the SpectraSyn Polyalphaolefin, was expected to yield small k_L values for both gases. On the other hand, the higher viscosity of Silicone Oil than that of the SpectraSyn Polyalphaolefin was expected to enhance the formation of large bubbles, resulting in small gas-liquid interfacial areas (a). This was true in the case of the light gas (He) where smaller k_L and, a values resulted in lower k_La values in the more viscous liquid (Silicone Oil). In the case of N_2, however, it seems that the induced heavy gas (N_2) bubbles were broken by the impeller and scattered throughout the reactor, leading to the formation of small bubbles with large gas-liquid

interfacial area (a).Thus, the small k_L values for N_2 in the more viscous Silicone Oil were overcame by its large a values, leading to higher k_La values.

6. Five liquids, namely Silicone oil, SpectraSyn polyalphaolefin, reactor wax, n-tetradecane and paraffins mixture, were investigated as potential startup liquids for F-T synthesis in SBCRs at 410 K and 15 bars for two values of α (0.92 and 0.85). This study indicated that the SpectraSyn polyalphaolefin could remain in the reactor for over 200 hr, whereas the Paraffins mixture would remain only for about 100 hr. This behavior was related to the molecular weight, which was the main factor controlling the residence time of the startup liquid in the SBCRs.

REFERENCES

[1] "World Energy Resources - 2013 Survey," World Energy Council2013.

[2] I. E. Agency, "World Energy Outlook 2011," 9 November 2011 2011.

[3] W. B. I. E. D. D. D. Group, *World development indicators*: World Bank, 2014.

[4] A. C. Vosloo, "Fischer-Tropsch: a futuristic view," *Fuel Processing Technology,* vol. 71, pp. 149-155, 2001.

[5] M. E. Dry, "Present and future applications of the Fischer-Tropsch process," *Applied Catalysis A: General,* vol. 276, pp. 1-3, 2004.

[6] D. J. Wilhelm, D. R. Simbeck, A. D. Karp, and R. L. Dickenson, "Syngas production for gas-to-liquids applications: technologies, issues and outlook," *Fuel Processing Technology,* vol. 71, pp. 139-148, 2001.

[7] G. Liu, E. D. Larson, R. H. Williams, T. G. Kreutz, and X. Guo, "Making Fischer−Tropsch Fuels and Electricity from Coal and Biomass: Performance and Cost Analysis," *Energy & Fuels,* vol. 25, pp. 415-437, 2011/01/20 2010.

[8] H. Schulz, "Short history and present trends of Fischer–Tropsch synthesis," *Applied Catalysis A: General,* vol. 186, pp. 3-12, 1999.

[9] D. Leckel, "Diesel Production from Fischer−Tropsch: The Past, the Present, and New Concepts," *Energy & Fuels,* vol. 23, pp. 2342-2358, 2009/05/21 2009.

[10] M. E. Dry, "The Fischer-Tropsch process: 1950-2000," *Catalysis Today,* vol. 71, pp. 227-241, 2002.

[11] A. Steynberg and M. Dry, *Fischer-Tropsch Technology*: Elsevier Science, 2004.

[12] C. L. Penniall, "Fischer-Tropsch Based Biomass to Liquid Fuel Plants in the New Zealand Wood Processing Industry Based on Microchannel Reactor Technology," 2013.

[13] Z. Liu, S. Shi, and Y. Li, "Coal liquefaction technologies—Development in China and challenges in chemical reaction engineering," *Chemical Engineering Science,* vol. 65, pp. 12-17, 2010.

[14] D. A. Wood, C. Nwaoha, and B. F. Towler, "Gas-to-liquids (GTL): A review of an industry offering several routes for monetizing natural gas," *Journal of Natural Gas Science and Engineering,* vol. 9, pp. 196-208, 2012.

[15] A. de Klerk, *Fischer-Tropsch Refining*. Weinheim: Wiley-VCH Verlag & Co. KGaA, 2012.

[16] F. G. Botes, J. W. Niemantsverdriet, and J. van de Loosdrecht, "A comparison of cobalt and iron based slurry phase Fischer–Tropsch synthesis," *Catalysis Today,* vol. 215, pp. 112-120, 2013.

[17] H. Schulz, G. Schaub, M. Claeys, and T. Riedel, "Transient initial kinetic regimes of Fischer–Tropsch synthesis," *Applied Catalysis A: General,* vol. 186, pp. 215-227, 1999.

[18] R. Deverell and M. Yu, "Long Run Commodity Prices: Where do we stand?," Credit Suisse27 July, 2011 2011.

[19] A.-G. Collot, "Matching gasification technologies to coal properties," *International Journal of Coal Geology,* vol. 65, pp. 191-212, 2006.

[20] R. L. Espinoza, a. P. Steynberg, B. Jager, and a. C. Vosloo, "Low temperature Fischer–Tropsch synthesis from a Sasol perspective," *Applied Catalysis A: General,* vol. 186, pp. 13-26, 1999.

[21] M. Dry, "The fischer-tropsch process-commercial aspects," *Catalysis today,* vol. 9570, 1990.

[22] J. Xu and G. Froment, "Methane steam reforming, methanation and water-gas shift: I. Intrinsic kinetics," *AIChE Journal,* vol. 35, pp. 88-96, 1989.

[23] W. Mitchell, J. Thijssen, and J. M. Bentley, "Development of a Catalytic Partial Oxidation/Ethanol Reformer for Fuel Cell Applications," *Society of Automotive Engineers,* vol. Paper No.9, 1995.

[24] M. Bradford and M. Vannice, "Catalytic reforming of methane with carbon dioxide over nickel catalysts II. Reaction kinetics," *Applied Catalysis A: General,* vol. 142, pp. 97-122, 1996.

[25] K. Kusakabe, K.-I. Sotowa, T. Eda, and Y. Iwamoto, "Methane steam reforming over Ce–ZrO_2-supported noble metal catalysts at low temperature," *Fuel Processing Technology,* vol. 86, pp. 319-326, 2004.

[26] a. Berman, R. K. Karn, and M. Epstein, "Kinetics of steam reforming of methane on Ru/Al_2O_3 catalyst promoted with Mn oxides," *Applied Catalysis A: General,* vol. 282, pp. 73-83, 2005.

[27] P. Wu, X. Li, S. Ji, B. Lang, F. Habimana, and C. Li, "Steam reforming of methane to hydrogen over Ni-based metal monolith catalysts," *Catalysis Today,* vol. 146, pp. 82-86, 2009.

[28] A. J. de Abreu, A. F. Lucrédio, and E. M. Assaf, "Ni catalyst on mixed support of CeO_2–ZrO_2 and Al_2O_3: Effect of composition of CeO_2–ZrO_2 solid solution on the methane steam reforming reaction," *Fuel Processing Technology,* vol. 102, pp. 140-145, 2012.

[29] H.-S. Roh, I.-H. Eum, and D.-W. Jeong, "Low temperature steam reforming of methane over Ni–$Ce_{(1-x)}Zr_{(x)}O_2$ catalysts under severe conditions," *Renewable Energy,* vol. 42, pp. 212-216, 2012.

[30] B. I. Morsi and O. Basha, "Indirect Coal Liquefaction," Antalyia, Turkey, 2014.

[31] G. J. V. R. R. Pandyala, M. Luo, B.H. Davis, "Fischer-Tropsch Synthesis: Effect of Start-Up Solvent in a Slurry Reactor," 2013.

[32] C. N. Satterfield and H. G. Stenger, "Effect of liquid composition on the slurry Fischer-Tropsch synthesis. 1. Rate of reaction," *Industrial & Engineering Chemistry Process Design and Development,* vol. 24, pp. 407-411, 1985/04/01 1985.

[33] B. H. Davis and E. Iglesia, "DOE Quarterly Report #8."

[34] R. J. Gormley, M. F. Zarochak, P. W. Deffenbaugh, and K. R. P. M. Rao, "Effect of initial was medium on the Fischer-Tropsch slurry reaction," *Applied Catalysis A: General,* vol. 161, pp. 263-279, 11/4/ 1997.

[35] C. M. White, K. L. Jensen, P. C. Rohar, J. P. Tamilia, L. J. Shaw, and R. F. Hickey, "Separation of Fischer−Tropsch Catalyst/Wax Mixtures Using Dense-Gas and Liquid Extraction," *Energy & Fuels,* vol. 10, pp. 1067-1073, 1996/01/01 1996.

[36] B. M. Karandikar, B. I. Morsi, Y. T. Shah, and N. L. Carr, "Effect of water on the solubilities and mass transfer coefficients of gases in a heavy fraction of fischer-tropsch products," *The Canadian Journal of Chemical Engineering,* vol. 65, pp. 973-981, 1987.

[37] B. M. Karandikar, B. I. Morsi, Y. T. Shah, and N. L. Carr, "Effect of water on the solubility and mass transfer coefficients of CO and H2 in a Fischer-Tropsch liquid," *The Chemical Engineering Journal,* vol. 33, pp. 157-168, 12// 1986.

[38] A. Deimling, B. M. Karandikar, Y. T. Shah, and N. L. Carr, "Solubility and mass transfer of CO and H2 in Fischer—Tropsch liquids and slurries," *The Chemical Engineering Journal,* vol. 29, pp. 127-140, 12// 1984.

[39] Y. T. Shah, *Gas-liquid-solid reactor design*: McGraw-Hill International Book Co., 1979.

[40] Y. T. Shah, B. G. Kelkar, S. P. Godbole, and W.-D. Deckwer, "Design parameters estimations for bubble column reactors," *AIChE Journal,* vol. 28, pp. 353-379, 1982.

[41] J. R. Inga and B. I. Morsi, "Effect of Operating Variables on the Gas Holdup in a Large-Scale Slurry Bubble Column Reactor Operating with an Organic Liquid Mixture," *Industrial & Engineering Chemistry Research,* vol. 38, pp. 928-937, 1999/03/01 1999.

[42] J. R. Inga and B. I. Morsi, "A Novel Approach for the Assessment of the Rate-Limiting Step in Fischer-Tropsch Slurry Process," *Energy & Fuels,* vol. 10, pp. 566-572, 1996/01/01 1996.

[43] E. Iglesia, "Design, synthesis, and use of cobalt-based Fischer-Tropsch synthesis catalysts," *Applied Catalysis A: General,* vol. 161, pp. 59-78, 1997.

[44] A. Akgerman, C. Erkey, and M. Orejuela, "Limiting Diffusion Coefficients of Heavy Molecular Weight Organic Contaminants in Supercritical Carbon Dioxide," *Industrial & Engineering Chemistry Research,* vol. 35, pp. 911-917, 1996/01/01 1996.

[45] M. A. Matthews and A. Akgerman, "Diffusion coefficients for binary alkane mixtures to 573 K and 3.5 MPa," *AIChE Journal,* vol. 33, pp. 881-885, 1987.

[46] M. A. Matthews, J. B. Rodden, and A. Akgerman, "High-temperature diffusion of hydrogen, carbon monoxide, and carbon dioxide in liquid n-heptane, n-dodecane, and n-hexadecane," *Journal of Chemical & Engineering Data,* vol. 32, pp. 319-322, 1987/07/01 1987.

[47] W. A. Marr, *History of Progress: Selected U.S. Papers in Geotechnical Engineering*: American Society of Civil Engineers, 2003.

[48] K. Muenz and J. M. Marchello, "Technique for Measuring Amplitudes of Small Surface Waves," *Review of Scientific Instruments,* vol. 35, pp. 953-957, 1964.

[49] G. Vázquez-Uña, F. Chenlo-Romero, M. Sánchez-Barral, and V. Pérez-Muñuzuri, "Mass transfer enhancement due to surface wave formation at a horizontal gas–liquid interface," *Chemical Engineering Science,* vol. 55, pp. 5851-5856, 12// 2000.

[50] J.-C. Charpentier, "Mass-Transfer Rates in Gas-Liquid Absorbers and Reactors," in *Advances in Chemical Engineering*. vol. Volume 11, G. R. C. J. W. H. Thomas B. Drew and V. Theodore, Eds., ed: Academic Press, 1981, pp. 1-133.

[51] M.-y. Chang and M. Badie I, "Mass transfer characteristics of gases in aqueous and organic liquids at elevated pressures and temperatures in agitated reactors," *Chemical Engineering Science,* vol. 46, pp. 2639-2650, // 1991.

[52] A. Behkish, "Hydrodynamic and Mass Transfer Parameters in Large-Scale Slurry Bubble Column Reactors," ed, 2004.

[53] P. V. Danckwerts, "Gas absorption accompanied by chemical reaction," *AIChE Journal,* vol. 1, pp. 456-463, 1955.

[54] G. Astarita, *Mass transfer with chemical reaction*: Elsevier, 1967.

[55] J. Charpentier, "Advances in chemical engineering," *Vol. II, Academic Press, New York,* 1981.

[56] Z. Tekie, J. Li, and B. I. Morsi, "Mass Transfer Parameters of O2 and N2 in Cyclohexane under Elevated Pressures and Temperatures: A Statistical Approach," *Industrial & Engineering Chemistry Research,* vol. 36, pp. 3879-3888, 1997.

[57] J. R. Inga and B. I. Morsi, "Effect of catalyst loading on gas/liquid mass transfer in a slurry reactor: a statistical experimental approach," *Canadian Journal of Chemical Engineering,* vol. 75, pp. 872-881, 1997.

[58] A. Deimling, B. M. Karandikar, Y. T. Shah, and N. L. Carr, "Solubility and mass transfer of carbon monoxide and hydrogen in Fischer-Tropsch liquids and slurries," *Chemical Engineering Journal (Amsterdam, Netherlands),* vol. 29, pp. 127-40, 1984.

[59] A. Lekhal, R. V. Chaudhari, A. M. Wilhelm, and H. Delmas, "Gas-liquid mass transfer in gas-liquid-liquid dispersions," *Chemical Engineering Science,* vol. 52, pp. 4069-4077, 1997.

[60] B. M. Karandikar, B. I. Morsi, Y. T. Shah, and N. L. Carr, "Effect of water on the solubilities and mass transfer coefficients of gases in a heavy fraction of Fischer-Tropsch products," *Canadian Journal of Chemical Engineering,* vol. 65, pp. 973-81, 1987.

[61] B. M. Karandikar, B. I. Morsi, Y. T. Shah, and N. L. Carr, "Effect of water on the solubility and mass transfer coefficients of CO and H2 in a Fischer-Tropsch liquid," *Chemical Engineering Journal (Amsterdam, Netherlands),* vol. 33, pp. 157-68, 1986.

[62] M. Y. Chang and B. I. Morsi, "Solubilities and mass transfer coefficients of carbon monoxide in a gas-inducing reactor operating with organic liquids under high pressures and temperatures," *Chemical Engineering Science,* vol. 47, pp. 3541-8, 1992.

[63] A. K. A. Alghamdi, "Mass transfer characteristics in a slurry agitated reactor with organic liquid mixtures under high pressures and temperatures," Unpublished M.S. Thesis, Chemical and Petroleum Engineering Department, University of Pittsburgh, Pittsburgh, 2001.

[64] H. Hichri, A. Accary, J. P. Puaux, and J. Andrieu, "Gas-liquid mass-transfer coefficients in a slurry batch reactor equipped with a self-gas-inducing agitator," *Industrial & Engineering Chemistry Research,* vol. 31, pp. 1864-7, 1992.

[65] R. S. Albal, Y. T. Shah, A. Schumpe, and N. L. Carr, "Mass transfer in multiphase agitated contactors," *Chemical Engineering Journal (Amsterdam, Netherlands),* vol. 27, pp. 61-80, 1983.

[66] R. S. Albal, Y. T. Shah, N. L. Carr, and A. T. Bell, "Mass transfer coefficients and solubilities for hydrogen and carbon monoxide under Fischer-Tropsch conditions," *Chemical Engineering Science,* vol. 39, pp. 905-7, 1984.

[67] E. Dietrich, C. Mathieu, H. Delmas, and J. Jenck, "Raney-nickel catalyzed hydrogenations: gas-liquid mass transfer in gas-induced stirred slurry reactors," *Chemical Engineering Science,* vol. 47, pp. 3597-604, 1992.

[68] S. A. Miller, A. Ekstrom, and N. R. Foster, "Solubility and mass-transfer coefficients for hydrogen and carbon monoxide in n-octacosane," *Journal of Chemical and Engineering Data,* vol. 35, pp. 125-7, 1990.

[69] J.-H. Chen, Y.-C. Hsu, Y. F. Chen, and C.-C. Lin, "Application of gas-inducing reactor to obtain high oxygen dissolution in aeration process," *Water Research,* vol. 37, pp. 2919-2928, 2003.

[70] S. Maalej, B. Benadda, and M. Otterbein, "Influence of pressure on the hydrodynamics and mass transfer parameters of an agitated bubble reactor," *Chemical Engineering & Technology,* vol. 24, pp. 77-84, 2001.

[71] Y.-C. Hsu, T.-Y. Chen, J.-H. Chen, and C.-W. Lay, "Ozone Transfer into Water in a Gas-Inducing Reactor," *Industrial & Engineering Chemistry Research,* vol. 41, pp. 120-127, 2002.

[72] Y.-C. Hsu, R. Y. Peng, and C.-J. Huang, "Onset of gas induction, power consumption, gas holdup and mass transfer in a new gas-induced reactor," *Chemical Engineering Science,* vol. 52, pp. 3883-3891, 1997.

[73] T. Sridhar and O. E. Potter, "Interfacial areas in gas-liquid stirred vessels," *Chemical Engineering Science,* vol. 35, pp. 683-95, 1980.

[74] S. Ledakowicz, H. Nettelhoff, and W. D. Deckwer, "Gas-liquid mass transfer data in a stirred autoclave reactor," *Industrial & Engineering Chemistry Fundamentals,* vol. 23, pp. 510-12, 1984.

[75] V. Linek, M. Kordac, M. Fujasova, and T. Moucha, "Gas-liquid mass transfer coefficient in stirred tanks interpreted through models of idealized eddy structure of turbulence in the bubble vicinity," *Chemical Engineering and Processing,* vol. 43, pp. 1511-1517, 2004.

[76] H. Hichri, A. Accary, J. P. Puaux, and J. Andrieu, "Gas-liquid mass-transfer coefficients in a slurry batch reactor equipped with a self-gas-inducing agitator," *Industrial & Engineering Chemistry Research,* vol. 31, pp. 1864-1867, 1992.

[77] T. Sridhar and O. E. Potter, "Interfacial areas in gas--liquid stirred vessels," *Chemical Engineering Science,* vol. 35, pp. 683-695, 1980.

[78] M. Teramoto, S. Tai, K. Nishii, and H. Teranishi, "Effects of pressure on liquid-phase mass transfer coefficients," *Chemical Engineering Journal (Amsterdam, Netherlands),* vol. 8, pp. 223-6, 1974.

[79] R. S. Albal, Y. T. Shah, A. Schumpe, and N. L. Carr, "Mass transfer in multiphase agitated contactors," *The Chemical Engineering Journal,* vol. 27, pp. 61-80, 1983.

[80] R. S. Albal, Y. T. Shah, N. L. Carr, and A. T. Bell, "Mass transfer coefficients and solubilities for hydrogen and carbon monoxide under Fischer-Tropsch conditions," *Chemical Engineering Science,* vol. 39, pp. 905-907, 1984.

[81] Z. Tekie, J. Li, and B. I. Morsi, "Mass Transfer Parameters of O_2 and N_2 in Cyclohexane under Elevated Pressures and Temperatures: A Statistical Approach," *Industrial & Engineering Chemistry Research,* vol. 36, pp. 3879-3888, 1997.

[82] S. A. Miller, A. Ekstrom, and N. R. Foster, "Solubility and mass-transfer coefficients for hydrogen and carbon monoxide in n-octacosane," *Journal of Chemical and Engineering Data,* vol. 35, pp. 125-127, 1990.

[83] B. M. Karandikar, B. I. Morsi, Y. T. Shah, and N. L. Carr, "Effect of water on the solubilities and mass transfer coefficients of gases in a heavy fraction of Fischer-Tropsch products," *Canadian Journal of Chemical Engineering,* vol. 65, pp. 973-981, 1987.

[84] M. Y. Chang and B. I. Morsi, "Solubilities and mass transfer coefficients of carbon monoxide in a gas-inducing reactor operating with organic liquids under high pressures and temperatures," *Chemical Engineering Science,* vol. 47, pp. 3541-3548, 1992.

[85] E. Dietrich, C. Mathieu, H. Delmas, and J. Jenck, "Raney-nickel catalyzed hydrogenations: Gas-liquid mass transfer in gas-induced stirred slurry reactors," *Chemical Engineering Science,* vol. 47, pp. 3597-3604, 1992.

[86] Y.-C. Hsu, R. Y. Peng, and C.-J. Huang, "Onset of gas induction, power consumption, gas holdup and mass transfer in a new gas-induced reactor," *Chemical Engineering Science,* vol. 52, pp. 3883-3891, 1997.

[87] S. Ledakowicz, H. Nettelhoff, and W. D. Deckwer, "Gas-liquid mass transfer data in a stirred autoclave reactor," *Industrial & Engineering Chemistry Fundamentals,* vol. 23, pp. 510-512, 1984.

[88] A. Lekhal, R. V. Chaudhari, A. M. Wilhelm, and H. Delmas, "Gas-liquid mass transfer in gas-liquid-liquid dispersions," *Chemical Engineering Science,* vol. 52, pp. 4069-4077, 1997.

[89] F. N. Tsai, S. H. Huang, H. M. Lin, and K. C. Chao, "Solubility of methane, ethane, and carbon dioxide in a Mobil Fischer-Tropsch wax and in n-paraffins," *Chemical Engineering Journal (Amsterdam, Netherlands),* vol. 38, pp. 41-6, 1988.

[90] A. Ghosh, W. G. Chapman, and R. N. French, "Gas solubility in hydrocarbons-a SAFT-based approach," *Fluid Phase Equilibria,* vol. 209, pp. 229-243, 2003.

[91] D. Ronze, P. Fongarland, I. Pitault, and M. Forissier, "Hydrogen solubility in straight run gas oil," *Chemical Engineering Science,* vol. 57, pp. 547-553, 2002.

[92] J. Tong, W. Gao, R. L. Robinson, Jr., and K. A. M. Gasem, "Solubilities of Nitrogen in Heavy Normal Paraffins from 323 to 423 K at Pressures to 18.0 MPa," *Journal of Chemical and Engineering Data,* vol. 44, pp. 784-787, 1999.

[93] J. Park, X. Yi, K. A. M. Gasem, and R. L. Robinson, Jr., "Solubilities of Carbon Monoxide in Aromatic Hydrocarbons at Temperatures from 323 to 433 K and Pressures to 23.3 MPa," *Journal of Chemical and Engineering Data,* vol. 40, pp. 245-7, 1995.

[94] J. Park, R. L. Robinson, Jr., and K. A. M. Gasem, "Solubilities of Hydrogen in Heavy Normal Paraffins at Temperatures from 323.2 to 423.2 K and Pressures to 17.4 MPa," *Journal of Chemical and Engineering Data,* vol. 40, pp. 241-4, 1995.

[95] J. S. Chou and K. C. Chao, "Solubility of synthesis and product gases in a Fischer-Tropsch SASOL wax," *Industrial & Engineering Chemistry Research,* vol. 31, pp. 621-3, 1992.

[96] D. S. Van Vuuren, J. R. Hunter, and M. D. Heydenrych, "The solubility of various gases in Fischer-Tropsch reactor wax," *Chemical Engineering Science,* vol. 43, pp. 1291-6, 1988.

[97] S. H. Huang, H. M. Lin, F. N. Tsai, and K. C. Chao, "Solubility of synthesis gases in heavy n-paraffins and Fischer-Tropsch wax," *Industrial & Engineering Chemistry Research,* vol. 27, pp. 162-9, 1988.

[98] J. S. Chou and K. C. Chao, "Correlation of synthesis gas solubility in n-paraffin solvents and Fischer-Tropsch waxes," *Fluid Phase Equilibria,* vol. 46, pp. 179-95, 1989.

[99] Y. N. Wang, Y. W. Li, L. Bai, Y. L. Zhao, and B. J. Zhang, "Correlation for gas-liquid equilibrium prediction in Fischer-Tropsch synthesis," *Fuel,* vol. 78, pp. 911-917, 1999.

[100] E. A. Campanella, "Correlation and prediction of synthesis gas solubility in n-paraffin systems," *Chemical Engineering & Technology,* vol. 20, pp. 371-377, 1997.

[101] B. A. Mandagaran and E. A. Campanella, "Correlation and prediction of gas solubility in heavy complex liquids," *Chemical Engineering & Technology,* vol. 16, pp. 399-404, 1993.

[102] J. S. Chou and K. C. Chao, "Solubility of synthesis and product gases in a Fischer-Tropsch SASOL wax," *Industrial & Engineering Chemistry Research,* vol. 31, pp. 621-623, 1992/02/01 1992.

[103] D. S. van Vuuren, J. R. Hunter, and M. D. Heydenrych, "The solubility of various gases in Fischer-Tropsch reactor wax," *Chemical Engineering Science,* vol. 43, pp. 1291-1296, 1988.

[104] W. Gao, R. L. Robinson, Jr., and K. A. M. Gasem, "High-Pressure Solubilities of Hydrogen, Nitrogen, and Carbon Monoxide in Dodecane from 344 to 410 K at Pressures to 13.2 MPa," *Journal of Chemical and Engineering Data,* vol. 44, pp. 130-132, 1999.

[105] S. H. Huang, H. M. Lin, and K. C. Chao, "Experimental investigation of synthesis gas solubility in Fischer-Tropsch reactor slurry," *Fluid Phase Equilibria,* vol. 36, pp. 141-148., 1987.

[106] E. A. Campanella, "Correlation of solubilities of carbon monoxide, carbon dioxide, and hydrogen in paraffins," *Journal of Chemical Engineering of Japan,* vol. 26, pp. 48-51, 1993.

[107] J. R. Inga, "Scaleup and Scaledown of Slurry Reactors: A New Methodology," Ph.D., Chemical and Petroleum Engineering Department, University of Pittsburgh, Pittsburgh, PA, 1997.

[108] A. Ghosh, W. G. Chapman, and R. N. French, "Gas solubility in hydrocarbons—a SAFT-based approach," *Fluid Phase Equilibria,* vol. 209, pp. 229-243, 2003.

[109] B. B. Breman, A. A. C. M. Beenackers, E. W. J. Rietjens, and R. J. H. Stege, "Gas-Liquid Solubilities of Carbon Monoxide, Carbon Dioxide,Hydrogen, Water, 1-Alcohols ($1 < n < 6$), and n-Paraffins ($2 < n < 6$) in Hexadecane, Octacosane, 1-Hexadecanol, Phenanthrene, and Tetraethylene Glycol at Pressures up to 5.5 MPa and Temperatures from 293 to 553 K," *Journal of Chemical and Engineering Data,* vol. 39, pp. 647-666, 1994.

[110] A. Behkish, Z. Men, J. R. Inga, and B. I. Morsi, "Mass transfer characteristics in a large-scale slurry bubble column reactor with organic liquid mixtures," *Chemical Engineering Science,* vol. 57, pp. 3307-3324., 2002.

[111] J. Tong, W. Gao, R. L. Robinson, and K. A. M. Gasem, "Solubilities of Nitrogen in Heavy Normal Paraffins from 323 to 423 K at Pressures to 18.0 MPa," *Journal of Chemical & Engineering Data,* vol. 44, pp. 784-787, 1999/07/01 1999.

[112] G. E. P. Box and N. R. Draper, *Empirical model-building and response surfaces*: Wiley, 1987.

[113] A. Behkish, R. Lemoine, L. Sehabiague, R. Oukaci, and B. I. Morsi, "Gas holdup and bubble size behavior in a large-scale slurry bubble column reactor operating with an organic liquid under elevated pressures and temperatures," *Chemical Engineering Journal,* vol. 128, pp. 69-84, 2007.

[114] R. Lemoine, A. Behkish, and B. I. Morsi, "Hydrodynamic and Mass-Transfer Characteristics in Organic Liquid Mixtures in a Large-Scale Bubble Column Reactor for the Toluene Oxidation Process," *Industrial & Engineering Chemistry Research,* vol. 43, pp. 6195-6212, 2004.

[115] L. Sehabiague, R. Lemoine, A. Behkish, Y. J. Heintz, M. Sanoja, R. Oukaci, *et al.*, "Modeling and optimization of a large-scale slurry bubble column reactor for producing 10,000bbl/day of Fischer–Tropsch liquid hydrocarbons," *Journal of the Chinese Institute of Chemical Engineers,* vol. 39, pp. 169-179, 2008.

[116] Z. Tekie, J. Li, B. I. Morsi, and M.-Y. Chang, "Gas-liquid mass transfer in cyclohexane oxidation process using gas-inducing and surface-aeration agitated reactors," *Chemical Engineering Science,* vol. 52, pp. 1541-1551, 1997.

[117] D. Saruhashi, B. Xiang, Z. Liu, and S. Yanabu, "Thermal degradation phenomena of flame resistance insulating paper and oils," *Dielectrics and Electrical Insulation, IEEE Transactions on,* vol. 20, pp. 122-127, 2013.

[118] K. Chenoweth, S. Cheung, A. C. T. van Duin, W. A. Goddard, and E. M. Kober, "Simulations on the Thermal Decomposition of a Poly(dimethylsiloxane) Polymer Using the ReaxFF Reactive Force Field," *Journal of the American Chemical Society,* vol. 127, pp. 7192-7202, 2005/05/01 2005.

[119] Sigma-Aldrich, "Silicone Oil - Dow Corning Corporation 200 Product Specification," ed.

[120] "Internal Communication."

[121] J. J. Marano and G. D. Holder, "General Equation for Correlating the Thermophysical Properties of n -Paraffins, n -Olefins, and Other Homologous Series. 2. Asymptotic Behavior Correlations for PVT Properties," *Industrial & Engineering Chemistry Research,* vol. 36, pp. 1895-1907, 1997.

[122] J. J. Marano and G. D. Holder, "A General Equation for Correlating the Thermophysical Properties of n -Paraffins, n -Olefins, and Other Homologous Series. 3. Asymptotic Behavior Correlations for Thermal and Transport Properties," *Industrial & Engineering Chemistry Research,* vol. 36, pp. 2399-2408, 1997.

[123] J. J. Marano and G. D. Holder, "General Equation for Correlating the Thermophysical Properties of n-Paraffins, n-Olefins, and Other Homologous Series. 1. Formalism for Developing Asymptotic Behavior Correlations," *Industrial & Engineering Chemistry Research,* vol. 36, pp. 1887-1894, 1997/05/01 1997.

[124] E. Ricci, R. Sangiorgi, and A. Passerone, "Density and surface tension of dioctylphthalate, silicone oil and their solutions," *Surface and Coatings Technology,* vol. 28, pp. 215-223, 6// 1986.

[125] C. R. Wilke and P. Chang, "Correlation of diffusion coefficients in dilute solutions," *AIChE Journal,* vol. 1, pp. 264-270., 1955.

[126] Y. Rakymkul, "Solubilities and Mass Transfer Coefficients of Gases in Heavy Synthetic Hydrocarbon Liquids," M.Sc., University of Pittsburgh, Pittsburgh, 2011.

[127] J. R. Inga, "Scaleup and Scaledown of Slurry Reactors: A New Methodology," ed, 1997.

[128] L. Sehabiague, "Modeling, Scaleup and Optimization of Slurry Bubble Column Reactors for Fischer-Tropsch Synthesis," Doctoral Dissertation, Department of Chemical and Petroleum Engineering, University of Pittsburgh, 2012.

[129] J.-p. Soriano, "Mass transfer characteristics in an agitated slurry reactor operating under Fischer-Tropsch conditions," University of Pittsburgh, 2005.

[130] A. P. Raje and B. H. Davis, "Effect of Vapor−Liquid Equilibrium on Fischer−Tropsch Hydrocarbon Selectivity for a Deactivating Catalyst in a Slurry Reactor," *Energy & Fuels,* vol. 10, pp. 552-560, 1996/01/01 1996.

[131] L. Caldwell and D. S. Van Vuuren, "On the formation and composition of the liquid phase in Fischer-Tropsch reactors," *Chemical Engineering Science,* vol. 41, pp. 89-96, 1986.